Development of a RET activity gene signature and a RET Antibody-Drug Conjugate

A THESIS SUBMITTED TO THE GRADUATE SCHOOL OF THE UNIVERSITY OF MINNESOTA BY

Saasha Vinoo

IN PARTIAL FULFILLMENT OF THE REQUIREMENTS FOR THE DEGREE OF MASTER OF SCIENCE

Advisor: Dr. Justin M Drake

May 2025

Acknowledgments

First and foremost, I would like to express my deepest gratitude to my advisor, Dr. Justin Drake, for his mentorship, guidance, and support throughout my master's journey. His scientific insight, patience, and encouragement have shaped my research and professional development.

I would also like to thank my thesis committee members, Dr. Hai Dang Nguyen and Dr. Justin Hwang for their valuable feedback, constructive critiques, and thought-provoking discussions which greatly improved the quality of this work.

I am sincerely grateful to Dr. Ali Arafa, Dr. Baishali Bhattacharya, Chau Dinh Quynh, and Gabi Larson whose collaboration and technical assistance created a supportive and intellectually stimulating environment. I want to thank Dr. Megan Ludwig, whose mentorship, scientific rigor, and constant encouragement have profoundly impacted my growth. Special thanks to Sachi Bhalchandra Tengse for being such a great lab mate and friend, with whom I shared troubleshooting sessions, and countless moments that made research more enjoyable.

Finally, I would like to acknowledge my family for their unconditional love, patience, and belief in me. To my parents and sister, your support has been the foundation of my academic journey, and I am forever thankful for your encouragement every step of the way.

Abstract

Neuroendocrine prostate cancer (NEPC) is an aggressive subtype of prostate cancer with limited treatment options and poor prognosis. The REarranged during Transfection (RET) receptor tyrosine kinase has emerged as a critical oncogenic driver in NEPC, with increased expression correlating with treatment resistance and disease progression. While RET-targeted therapies have shown to target RET fusions and RET kinase inhibitors have proven efficient in other cancer types such as medullary thyroid cancers, there is an urgent need for biomarker-specific approaches. To address this gap, we propose two strategies: (1) defining a RET activity signature to stratify NEPC patients most likely to benefit from RET inhibition therapies, and (2) developing a RET-targeted antibody-drug conjugate (ADC).

To define a RET activity signature, we characterize transcriptional changes driven by RET expression. RNA sequencing of RET knockdown and overexpression models will identify key gene networks associated with RET expressions. Integration of this data will generate a functional RET signature, which will be evaluated as a potential biomarker for NEPC.

In parallel, we are working on a novel RET ADC, in which a RET-targeting single-chain fragment variable (scFv) is conjugated to the topoisomerase-1 inhibitor SN-38 via optimized cleavable linkers. This approach leverages the selective overexpression of RET in NEPC to deliver cytotoxic payloads directly to tumor cells, thereby minimizing off-target toxicity. Together, these studies aim to establish RET as both a predictive biomarker as well as a therapeutic target in NEPC that improves patient outcomes in this cancer.

Table of Contents

Acknowledgments…….……i

Abstract……..ii

Table of Contents……...…….iii

List of Tables...……...…….iv

List of Figures..……...……...……v

Chapter I: Generation of an mRNA gene signature……...……1

Sub-Chapter I: Introduction……...…….2

Sub-ChapterII: Materials and Methods……...……11

Sub-Chapter III: Results……16

Chapter II: Generation of a RET targeted Antibody-Drug Conjugate…..……...……23

Sub-Chapter I: Introduction……..24

Sub-Chapter II: Materials and Methods……...……...29

Sub-Chapter III: Results……..…..36

Chapter III: Discussion……...……...……42

Chapter IV: Failed Experiments and Troubleshooting……..……46

Chapter V: Future Directions……..……...…..52

Bibliography……..…..55

List of Tables

Table 1: List of Prostate and Lung Cancer Cell Lines……...…….11

Table 2: RIN scores of prostate and lung cancer cell lines……..22

List of Figures

Figure 1: New Cancer Cases Estimated in 2025……..2

Figure 2: Progression of Prostate Cancer……...4

Figure 3: Development of NEPC……...6

Figure 4: Experimental flow for generating mRNA gene signature……...15

Figure 5: Cell line panel of prostate and lung cancer cell lines after RET overexpression……..17

Figure 6: Cell line panel of prostate cancer cell line after knocking down RET……...20

Figure 7: Structure of an ADC……...24

Figure 8: Mechanism of action of our RET-targeted ADC……..26

Figure 9: Experimental flow for the RET ADC project……..35

Figure 10: Coomassie stain blots for scFv visualization……..37

Figure 11: Western blots for scFv visualization using His-Tagged antibody……37

Figure 12: Flow cytometry results to show binding between RET+ cells and the scFv...39

Figure 13: Wild-type shRNA transduction in DMS53 and SHP77……...47

Figure 14: siRNA transfection in lung cancer cell lines using lipofectamine……48

Figure 15: siRNA transfection in lung cancer cell lines using TransIT…...……..48

Figure 16: SDS PAGE after fast IPTG induction……49

Figure 17: SDS PAGE showing induction using different IPTG ranges……...…50

Figure 18: Western blot showing IPTG induction……...50

Figure 19: Western blot quantification to optimize osmotic shock buffer (By Megan)...51

CHAPTER I

Generation of an mRNA gene signature

SUB-CHAPTER I: Introduction

Prostate Cancer Statistics

Prostate cancer (PCa) is among the most common cancers in men globally and ranks as the second leading cause of cancer-related mortality after lung cancer. In 2025, an estimated 313,780 new cases are expected to be diagnosed in the United States, with around 64,190 projected deaths (Figure1). [1]

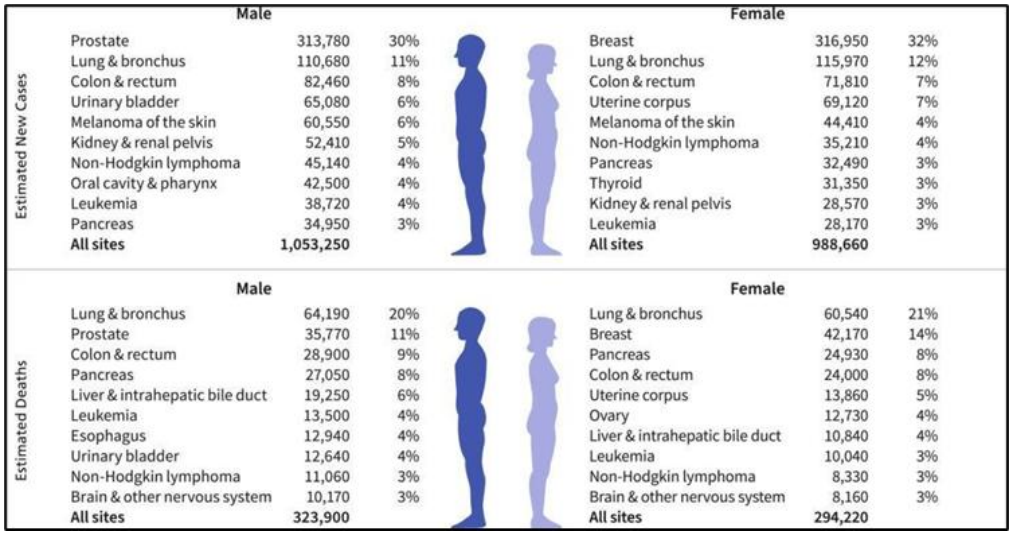

Figure 1: Prostate Cancer Statistics. New Cancer Cases Estimated in 2025 [1] Prostate Cancer will make up 30% of new estimated cancer cases and 11% of estimated cancer deaths in men in 2025.

It is derived from the epithelial cells of the prostate gland and manifests a wide range of clinical characteristics, starting from slow-growing tumors to aggressive, metastatic illness.[2] Age is a major risk factor, with over 60% of cases occurring in men aged 65 and older. Early detection can improve outcomes, with localized and regional cases having a nearly 100% five-year relative survival rate. However, survival drops sharply to around 30% for metastatic prostate cancer. The

widespread adoption of PSA testing has significantly reduced mortality rates over the past decade, but recent data suggests this decline has leveled off, potentially due to an increase in late-stage diagnoses. Early-stage prostate cancer frequently has no symptoms and progresses slowly, requiring little or no treatment. The most common complaint is nocturia, increased frequency, and difficulty urinating, all of which can also be caused by prostatic enlargement. [2]

Prostate Cancer Treatment and Progression

For men diagnosed with metastatic or recurrent prostate cancer, the primary treatment approach is Androgen Deprivation Therapy (ADT). Adenocarcinomas, which account for most prostate malignancies, initially depend on androgen receptor (AR) signaling for their growth and survival. Therefore, a crucial aspect of treating advanced illness has been ADT. [3]

Prostate cancer advances due to genetic and epigenetic changes that encourage unchecked cell division and treatment resistance. Mutations in tumor suppressor genes like *TP53* and *PTEN* the activation of oncogenic pathways like PI3K/AKT/mTOR, and chromosomal rearrangements are examples of important molecular alterations. ERG fusions, most commonly *TMPRSS2-ERG* are early events in prostate tumorigenesis that promote oncogenic transcriptional programs and enhance cellular invasion.[4] *MYC* amplifications are frequently observed in advanced disease and metastatic prostate cancer, where increased MYC expression drives proliferation, metabolic reprogramming, and tumor aggressiveness.[5] While surgery or radiation therapy can often be used to effectively control localized prostate cancer, the advanced illness commonly progresses to castration-resistant prostate cancer (CRPC) upon resistance to first-generation ADT and it is more likely to spread. [6] AR mutations, particularly those affecting the ligand-binding domain, enable

cancer cells to sustain androgen receptor signaling even under low-androgen conditions, contributing to CRPC.[7]

Standard treatment options for CRPC include second-generation hormonal therapies such as enzalutamide,[8] which inhibit the androgen receptor pathway, and androgen biosynthesis inhibitors like abiraterone acetate, which suppresses testosterone production.

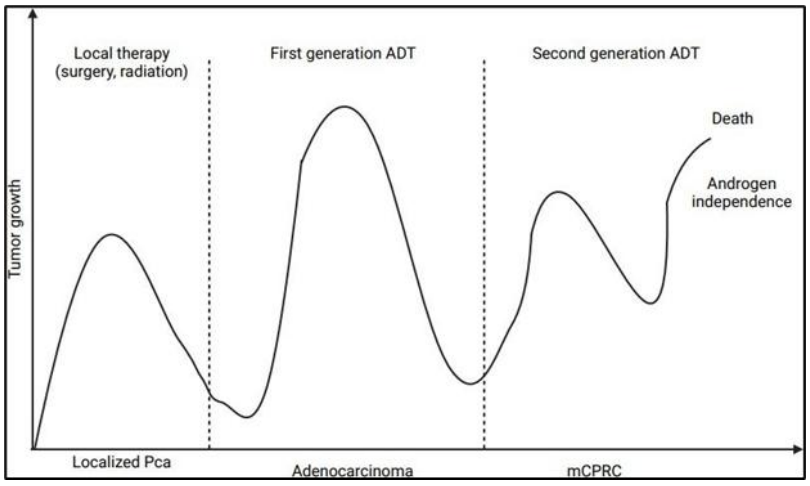

Figure 2: Progression of Prostate Cancer. Surgery and radiation therapy are available treatment options for localized prostate cancer. As this advances into adenocarcinoma, first-generation ADTs are utilized. The cancer cells might progress into mCRPC due to resistance ADTs during which second-generation ADTs are given to patients. The cancer can then progress to an Aggressive Variant Prostate Cancer, which does not have a targeted therapy.

Despite initial response to these treatments, some patients eventually develop AR signaling-negative tumors, classified as aggressive variant prostate cancer (AVPC). Although AVPC accounts for less than 1% of primary prostate cancer cases [8], it is observed in approximately 25-35% of CRPC cases that have been treated with second-generation hormonal therapies. The treatment of prostate cancer has changed as a result of recent developments in molecular profiling

and targeted medicines. Patient outcomes have improved as a result of the discovery of molecular subtypes, the emergence of new AR inhibitors, and the advent of precision medicine techniques, such as PARP inhibitors for tumors with altered homologous DNA repair.[8,10] Treatment resistance is still a problem, though, particularly in aggressive forms like NEPC, which emphasizes the necessity of more research into biomarkers, therapeutic targets, and individualized treatment plans. [9]

Neuroendocrine Prostate Cancer (NEPC)

AVPC tumors can be classified into two primary molecular subtypes: double-negative prostate cancer (DNPC) and neuroendocrine prostate cancer (NEPC). The loss of androgen receptor (AR) signaling and the development of neuroendocrine (NE) characteristics define NEPC, an uncommon but aggressive subtype of prostate cancer.[10,11] In contrast to traditional prostate adenocarcinoma, NEPC expresses markers (such as synaptophysin, chromogranin A, and neuron-specific enolase), has small- or large-cell neuroendocrine architecture, and is frequently linked to a poor prognosis.[12] Genetic and epigenetic changes that promote lineage plasticity are what give rise to NEPC. These changes allow prostate cancer cells to differentiate into a neuroendocrine state in response to selection pressure from AR-targeted treatments. Deregulation of MYCN and EZH2, and activation of stemness pathways, are important molecular drivers.[12] The lethality of NEPC is attributed to its strong capacity for metastasis and rapid proliferation; patients frequently appear with visceral metastases and have a poor response to standard hormone treatments. [13]

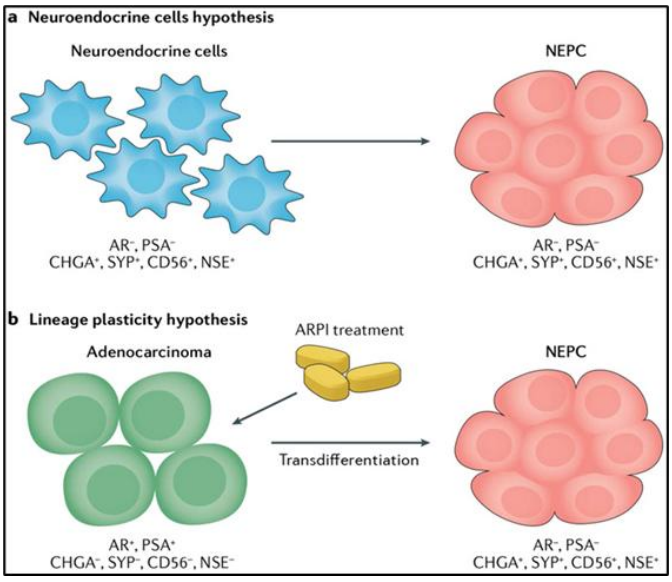

Figure 3: Development of NEPC [7]. Treatment-Emergent NEPC is when the tumors are resistant to ADTs. De novo NEPC can arise from NEPC epithelial cells.

While there is currently no cure for NEPC, platinum-based chemotherapy is commonly used as the first-line treatment and is sometimes combined with taxanes. However, although some patients initially respond to treatment, the duration of this response is often short-lived.[14] Novel diagnostic, prognostic, and therapeutic approaches are needed considering the rising clinical incidence of therapy-induced NEPC. Finding biomarkers for early detection, comprehending the processes behind neuroendocrine transdifferentiation, and investigating tailored treatments that target the particular vulnerabilities of NEPC cells are the main goals of current research initiatives.[15]

RET Receptor Tyrosine Kinase

The receptor tyrosine kinase encoded by the RET proto-oncogene is essential for kidney and nervous system development. Normal cellular differentiation, proliferation, and survival depend

on RET signaling; nevertheless, several malignancies have been linked to dysregulation of the RET pathway caused by mutations, fusions, or overexpression.[16] The Drake laboratory's recent research has identified RET as a key factor in tumor growth and treatment resistance in the setting of prostate cancer, especially aggressive variants like NEPC.[17] AR-independent (NEPC) and AR-dependent prostate cancer cell lines were compared using a thorough phosphoproteomic analysis, which showed that AR-independent cells have much higher levels of RET kinase activity. Moreover, RET's functional significance in maintaining these tumors was highlighted by the fact that RET inhibition in NEPC models, whether genetic or pharmacologic, led to decreased tumor growth and increased cell death. [18]

Prostate cancer is not the only cancer where RET is overexpressed. KIF5B-RET and other RET gene fusions have been found in 1-2 percent of Non-small cell lung cancer adenocarcinomas. These changes make tumors more susceptible to selective RET inhibitors, which have had encouraging results in clinical trials.[19] Furthermore, the application of RET inhibitors such as pralsetinib (BLU-667) and selpercatinib (LOXO-292) has produced noteworthy clinical responses in lung tumors with RET alterations (i.e. fusions and point mutations), indicating the therapeutic potential of RET targeting across cancer types.[20]

Determining RET's carcinogenic function has been made possible by preclinical models, such as lung adenocarcinoma and prostate cancer cell lines like NCI-H660. In NCI-H660 cells, RET knockdown or inhibition reduced downstream MAPK and PI3K/AKT signaling, which led to decreased proliferation in prostate cancer. Similarly, *both in vitro and in vivo*, RET- dependent lung cancer cells have a high level of sensitivity to RET inhibitors.[18,]

Understanding RET signaling in various cellular contexts is essential given the increasing awareness of RET as an oncogenic driver and its developing involvement in therapy resistance, particularly in lineages like prostate and lung malignancies that are susceptible to treatment-induced plasticity. In order to identify RET's role in tumor progression and evaluate the therapeutic potential of RET inhibition in models with enhanced RET activity, we will examine the expression, modulation, and functional relevance of RET in prostate and lung cancer cell lines.

Small Cell Lung Cancer

Small cell lung cancer (SCLC) accounts for roughly 10–15% of all cases and lung cancer continues to be the primary cause of cancer-related fatalities globally. Although SCLC is less common than non-small cell lung cancer (NSCLC), it is a particularly aggressive subtype that is marked by early metastases, fast tumor growth, and a strong correlation with tobacco use. According to histology, SCLC is a high-grade neuroendocrine carcinoma. It usually consists of tiny, round to spindle-shaped cells with finely granular chromatin and little cytoplasm. Although SCLC is known for its initial sensitivity to radiation and chemotherapy, recurrence and the emergence of treatment resistance are common features of clinical history.[22,23]

Histologically, SCLC exhibits poorly differentiated neuroendocrine features, consistent with its origin from neuroendocrine cells in the lung. The majority of patients are diagnosed with advanced stages of the disease, and the median overall survival is still less than a year, underscoring the pressing need for novel treatment strategies.[24] The tumor suppressor genes TP53 and RB1 are almost universally inactivated in SCLC, whereas oncogenes such as MYC, SOX2, and BCL2 are frequently amplified or overexpressed.[25] The subclassification of SCLC

into molecular subtypes based on transcription factor expression has also been made possible by recent developments in high-throughput sequencing and transcriptomic profiling. These subtypes include ASCL1, NEUROD1, POU2F3, and YAP1, each of which may represent unique cells of origin and therapeutic vulnerabilities.[25,26] RET plays an emerging oncogenic role in small-cell lung cancer (SCLC), with the identification of activating RET mutations in metastatic SCLC tumors. Overexpression of both wild-type and mutant RET in SCLC cell lines led to enhanced ERK signaling, MYC expression, and increased proliferation. Importantly, RET-overexpressing cells showed sensitivity to RET-targeted tyrosine kinase inhibitors like vandetanib.[26] Given these shared features, our research will be expanded to include studies on SCLC.

Non-small cell lung cancer

About 85–90% of all lung cancer cases are non-small cell lung cancer (NSCLC), a diverse group of cancers that originate from the lung's epithelial cells. Despite advancements in early identification and treatment, NSCLC remains a major cause of cancer-related death globally, typically manifesting at an advanced stage. Historically, treatment options for NSCLC were limited to cytotoxic chemotherapy and radiation.[27] Numerous driver mutations and oncogenic changes in NSCLC have been identified through genomic profiling. These changes include mutations in EGFR, ALK, KRAS, ROS1, BRAF, RET, and MET, among others. As a result of these findings, personalized treatment plans that consider each tumor's unique molecular profile have been developed. Tyrosine kinase inhibitors (TKIs) specifically targeting ALK and EGFR have demonstrated significant clinical benefits in certain patient groups.[28]

Despite these advancements, challenges remain in overcoming acquired and primary resistance to

immunotherapies and targeted therapies. Understanding the molecular mechanisms underlying tumor growth, heterogeneity, and resistance is essential to improve patient outcomes.[29]

We chose to include this cancer type to enhance RET expression diversity–by studying both high RET-expressing and low RET-expressing cell lines, the study can better capture genes directly associated with RET activity. By assessing how RET suppression or overexpression affects transcriptional changes across different cell lines, we can refine the RET activity signature to focus on genes consistently regulated by RET rather than non-specific changes observed in a single cancer type.

SUB-CHAPTER II: MATERIALS AND METHODS

2.1 Cell lines chosen for the project

Various prostate adenocarcinoma, neuroendocrine prostate cancer, small cell lung cancer, and non-small lung cancer cell lines were chosen namely- 22Rv1, PC3, NCI H660, LASCPC-01, SHP-77, DMS53, NCIH1435, and NCIH1650, and are summarized below. (Table 1)

Cell line	Mutation	Characteristics
NCIH660	TP53 (inactivated), PTEN (inactivated), RB1 (inactivated)	Presence of ASCL1, NSE, SYP, BRN2, SOX2, FOXA1, high expression of Ki-67
LASCPC-01	TP53 (inactivated), RB1(inactivated), PTEN (inactivated)	N-Myc is the driver of NEPC. Presence of ASCL1, NSE. Activated AKT1 and AURKA
PC3	TP53 (inactivated), PTEN (inactivated), RB1 (inactivated), (activating), p21 (lower expression due to TP53 mutation)	Presence of CHA, FOXA1, CD44, NSE, focal positivity for CK8, AR detected at mRNA level, activated PI3K/AKT pathway
22Rv1	PIK3CA (activated), AR (expression of AR splice variants like AR-V7), TP53 (partially inactivated)	Presence of NSE, high ERK activation seen
DMS53	TP53 (inactivated), RB1(inactivated), PTEN(inactivated)	Expression of MYC,ASCL1, NEUROD1 and exhibits NE features
SHP77	TP53(inactivated), RB1(inactivated)	Unusual undifferentiated large cell variant of SCLC, CD56 antigen and ASCL1,NCAM1 expression
NCI H1650	TP53(inactivated), BRAF(activated), RB1(inactivated), CDKN2A(inactivated), PTEN(inactivated)	Expression of E-Cadherin, stem cell markers like Oct-4, AKT, and ERK phosphorylation
NCIH1435	TP53 (inactivated), PIK3CA (activated), KEAP1 (inactivated)	Expresses epithelial markers like CDH1

Table 1: List of prostate and lung cancer cell lines.

2.2 Cell Culture

22Rv1, PC3, NCI H660, LASCPC-01, SHP-77, DMS53, and NCIH1650 cell lines were purchased from ATCC. The NCIH1435 cell lines were a gift from Dr. Robert Kratzke at the University of Minnesota. The 22Rv1, PC3, SHP-77, DMS53, NCIH1435, and NCIH1650 cell lines were cultured in RPMI 1640 (Gibco) medium supplemented with 10% Fetal Bovine Serum (Sigma Aldrich) and 1% Penicillin- Streptomycin (Life Technologies). The LASCPC-01 and NCI-H660 cell lines were cultured in Advanced DMEM/F12 (Gibco) medium supplemented with 1× B27 Supplement (Gibco), 10 ng/mL EGF (PeproTech), 10 ng/mL bFGF (PeproTech), 1% penicillin–streptomycin and 1× Glutamax (Life Technologies). All cell lines were maintained in incubators at 37°C and 5% CO_2. Mycoplasma checks using polymerase chain reaction methods were done routinely.

2.3 Generation of stable RET overexpression and knockdown Cell Lines

The pLKO.1 scramble shRNA plasmid was a gift from David Sabatini (Addgene plasmid). Two pLKO.1 –shRET plasmids were used to generate the knockdown cell lines were kindly provided by the laboratory of Dr. William C. Hahn (Dana-Farber Cancer Institute, Boston, MA) from the RNAi Consortium at the Broad Institute. Lentiviral particles were produced by transfecting 293T cells with 13µg pMDL, 5µg pRev, 7µg pVSVg and 20ug pLKO.1

shRNA plasmid using calcium chloride. Then the cells were transduced with lentivirus in media containing 8 μg/mL polybrene (Sigma-Aldrich). After 72 hours of infection, puromycin was used to select the stable cells. Similarly, for overexpression models, 20ug retroviral plasmid, 15ug pGag-Pol, and 5ug pVSVg were used for retrovirus production. The latter steps that followed were similar as the knockdown models.

2.4 Cell lysate isolation and Western Blotting

Cells were lysed in 2% SDS supplemented with 1X cOmplete Mini Protease Inhibitor Cocktail (Roche) and 1X Halt Phosphatase Inhibitor Single-Use Cocktail (Thermo). Protein concentrations were measured using the Pierce BCA Assay (Thermo). Before the analysis, the samples were boiled for five minutes at 95°C with a 5X loading buffer. Samples were run for 90 minutes at 100V at room temperature on 4–20% Mini-PROTEAN TGX Stain-Free protein gels. PVDF membranes having a pore size of 0.45μm (Millipore-Sigma) were used for the transfer, which was done overnight at 30V at 4°C. The membranes were blocked with 5% BSA in 1X TBS for 30 minutes at room temperature and incubated overnight at 4°C with primary antibodies diluted in 1% BSA in 1X TBST. Membranes were washed thrice with 1X TBST, incubated with Li-Cor IRDye Secondary Antibodies (1:5000 dilution) in the dark for 1 hour at room temperature. The membranes were washed thrice with 1X TBST and imaged using the Bio-Rad ChemiDoc MP Imaging System. Channels 700 and 800 were used to detect the mouse and rabbit secondary antibodies respectively. The following antibodies were used at a dilution of 1:1000 unless otherwise indicated. RET (Cell Signaling Technology 14556), AKT (Cell Signaling Technology 4691), ERK1/2 (Cell Signaling Technology 9102), P70S6K (Cell

Signaling Technology 2708), STAT3 (Cell Signaling Technology 9139), pRET Y1062 (Invitrogen PA5-104769), pRET Y905 (Cell Signaling Technology 3221), pAKT S473 (Cell Signaling Technology 4060), pERK1/2 T202/Y204 (Cell Signaling Technology 4370) 1:2000 dilution, pP70S6K T421/S424 (Cell Signaling Technology 9204), pSTAT3 Y705 (Cell Signaling Technology 9145), GAPDH (Genetex 239) and β-Actin (Santa Cruz Biotechnology 4778). GAPDH and β-Actin were used as loading controls. The experiments were performed in triplicates.

2.5 RNA isolation and RNA QC

RNA was isolated from the cells using the RNeasy Plus Mini Kit (50) by Qiagen. RNA isolation was performed in triplicates. The samples were then sent to the University of Minnesota Genomics Center to check for RIN (RNA integrity number) scores using Agilent. Samples having an RIN score of 4 and above were sent for sequencing.

2.6 qPCR

A NanoDrop spectrophotometer was used to check the concentration and purity of RNA. Complementary DNA (cDNA) was synthesized from 200 ng of RNA using the Maxima H Minus cDNA Synthesis Master Mix with dsDNAse by Thermo scientific according to the manufacturer's instructions. qPCR was performed using GoTaq qPCR Master Mix by Promega on an Applied Biosystems QuantStudio 3 Real Time PCR System with gene-specific primers by Biorad and IDT for RET gene and GAPDH as an internal control, respectively. The qPCR reactions were run in triplicate, and relative gene expression levels were analyzed

using the 2^−ΔΔCt method.

2.9 Statistical Analyses

Statistical analyses were performed with Graphpad Prism v.10 software.

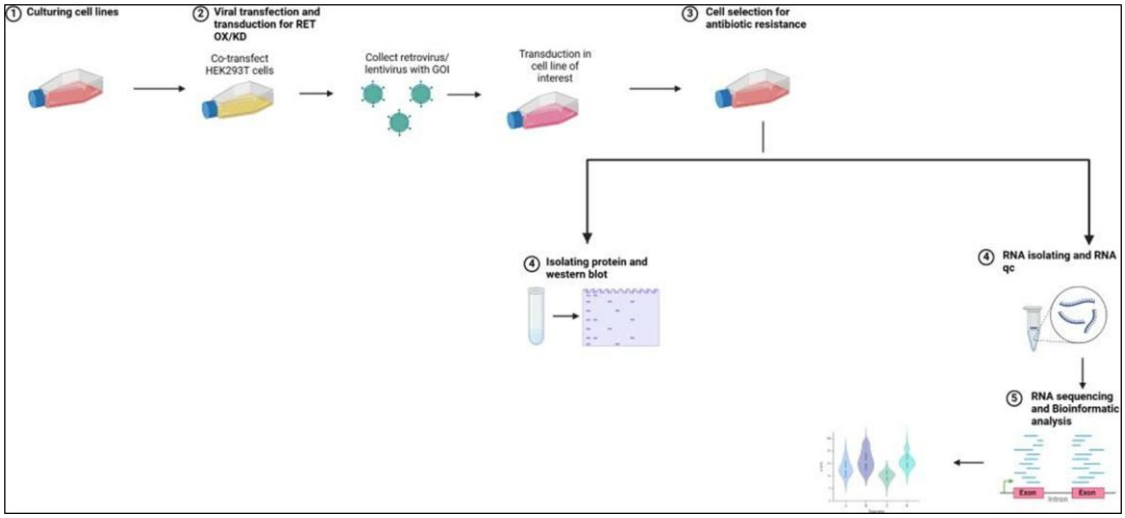

Figure 4: Experimental flow for generating mRNA gene signature. After culturing cell lines, HEK 293T cells were used for transfection followed by viral transduction on the cell lines of interest. Puromycin was used for selecting the cells with antibiotic resistance. Cells were lysed and western blots were used for preliminary testing of protein expression. RNA was isolated and RIN scores were calculated. These samples will then be sent to Novogene for mRNA sequencing.

SUBCHAPTER III: RESULTS

3.1 RET Overexpression in prostate and NSCLC cell lines

To define a functional RET transcriptional signature, we first generated cell line models with RET knockdown or RET overexpression across prostate and lung cancer cell lines differing in baseline RET expression. NCI-H660, LASCPC-01, DMS53, and SHP77 cell lines with high endogenous RET levels, were transduced with shRNA lentiviral vectors targeting RET, while PC-3, 22Rv1, H1435, and H1650 which lack endogenous RET expression, were stably transduced with retroviral vectors to overexpress RET. Our goal is to comprehend how RET alteration impacts the expression of its downstream proteins in cell line models for lung and prostate cancer. Figure 5A shows RET, phosphorylated RET, and downstream proteins such as STAT3, P70-S6 Kinase 1, AKT, ERK, and their phosphorylated counterparts in prostate cancer cell lines: PC3 and 22Rv1 after transduction and puromycin selection. NCI-H660 is positive control. In Figure 5B and 5C we tried to see if different media conditions play a role in phosphorylation patterns. Varying percentages of FBS in values of 10%, 5%, 2.5%, and 1% were used. We also used charcoal-stripped FBS media which mimics androgen depleted conditions in cell culture. Although not pronounced, increasing FBS concentration gives higher phosphorylation of RET and its downstream targets in PC3. 22Rv1 is an adenocarcinoma cell line with the presence of AR splice variants. In comparison, the PC3 cell line which shows the presence of various NE features seemed like a better cell line for RNA sequencing. Figure 5D shows RET, phosphorylated RET, and downstream proteins in non-small cell lung cancer cell line, H1650. This cell line harbors an EGFR mutation, which could

be one of the reasons there was not any difference in the phosphorylation patterns of the treatment versus the GFP control. Several compensatory mechanisms tend to be activated leading to the phosphorylation of kinases. H1435 cell line, which is also a non-small cell lung cancer cell line shows no difference in phosphorylation patterns in the control vs treatment group. Due to these reasons, they were not sent for RNA sequencing.

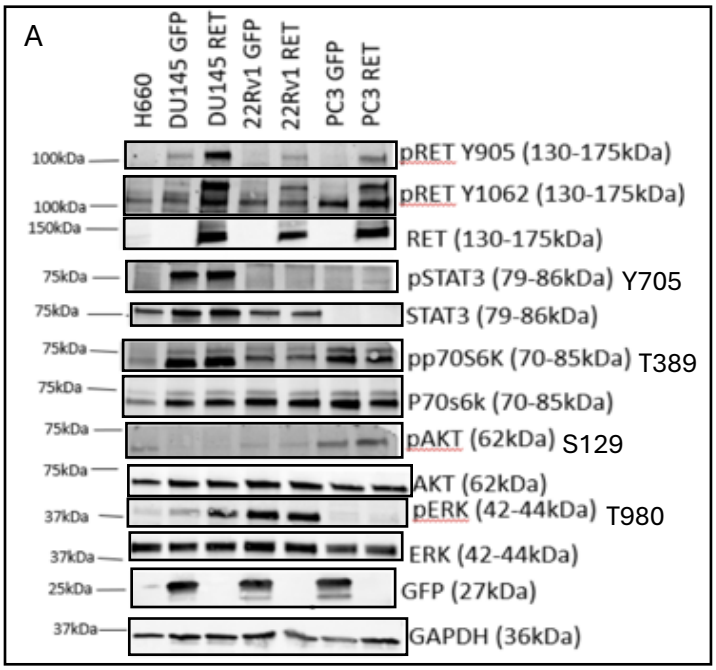

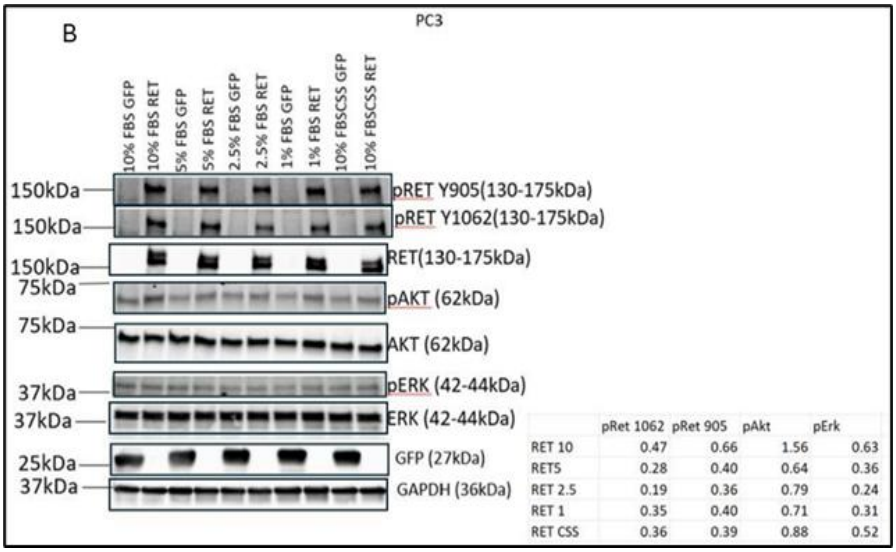

	pRet 1062	pRet 905	pAkt	pErk
RET 10	0.47	0.66	1.56	0.63
RET5	0.28	0.40	0.64	0.36
RET 2.5	0.19	0.36	0.79	0.24
RET 1	0.35	0.40	0.71	0.31
RET CSS	0.36	0.39	0.88	0.52

C

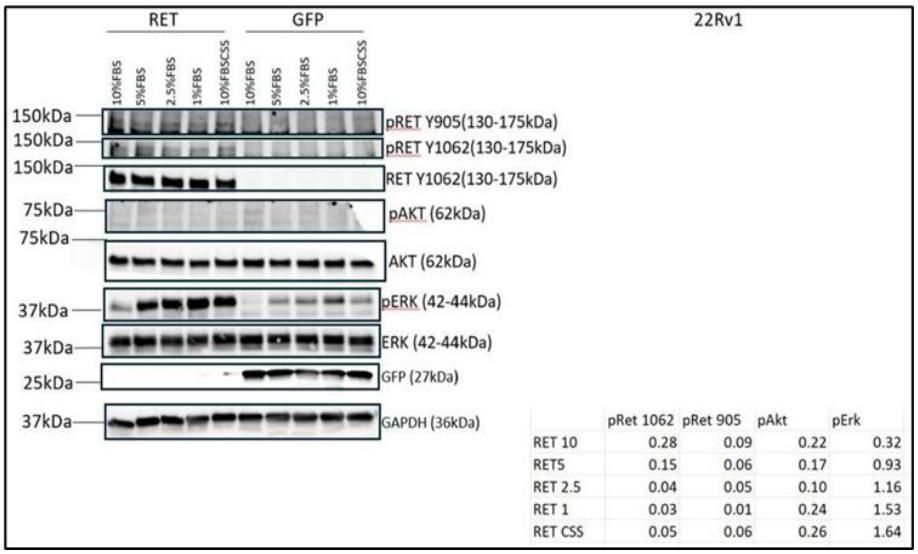

	pRet 1062	pRet 905	pAkt	pErk
RET 10	0.28	0.09	0.22	0.32
RET5	0.15	0.06	0.17	0.93
RET 2.5	0.04	0.05	0.10	1.16
RET 1	0.03	0.01	0.24	1.53
RET CSS	0.05	0.06	0.26	1.64

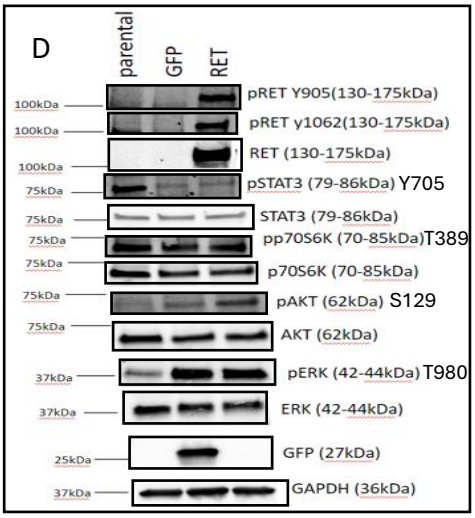

Figure 5: Cell line panel of prostate and lung cancer cell lines after overexpressing RET.

A. Western blots on prostate adenocarcinoma cell lines PC3 and 22Rv1 after retroviral transduction to overexpress RET showing activation of total and phosphorylated proteins. GFP is the transduction control and GAPDH is the loading control. B and C. Western blot upon using different concentrations of FBS in PC3 and 22Rv1 cell lines. D. Western blot showing activation of RET, its phosphorylated counterparts, and downstream targets in the H1650 cell line.

3.2 Knockdown of RET in NEPC and SCLC cell lines

NEPC cell lines H660 and LASCOC-01 were initially chosen for this study. We used the doxycycline-induced RET knockdown in H660. The scrambled control plasmid used was designed to be doxycycline-inducible, however, upon further analysis, I discovered that the puromycin resistance was absent. As a result, I could not select successfully transduced cells, which likely compromised the expression and functionality of the construct. Figure 6A shows the doxycycline-inducible shRNA blots and Figure 6B was graphed on GraphPad Prism after running a qPCR and comparing the gene expression of various treatments with H660 parental. H660 p denotes the parental cell line, h660 s stands for scrambled control without doxycycline, h660 sd represents scrambled control with addition of doxycycline, h660 r is shRET without addition of doxycycline and h660 rd is the shRET construct with the addition of doxycycline. The Ct values along with the standard deviation of the fold difference was plotted on GraphPad Prism. From the western blots and qPCR data it is evident that transducing the cells with the shRET construct virus leads to a RET knockdown, although more pronounced after the addition of doxycycline. Since the shscr with doxycycline inducible system could not be expanded for a long time, wild type shRET was used. Fig 6C shows a knockdown of RET using wildtype transduction. For the knockdown models as well, not much of a difference was seen in the phosphorylation patterns of downstream targets as seen in Fig 6D. This points to the fact that other non-canonical pathways are also activating the various kinases. Fig 6E shows a qPCR of the H660 parental cell line along with different treatment conditions including 2 scrambled and 2 RET knockdown conditions. Western blots and qPCR data show that ~70% knockdown was achieved relative to scrambled shRNA controls. We got a robust reduction of RET protein levels in RET-positive lines and strong upregulation of RET protein in

RET- negative models. These biochemical validations gave the desired overexpression or knockdown for RET, but they did not shed much light on its downstream activity.

A

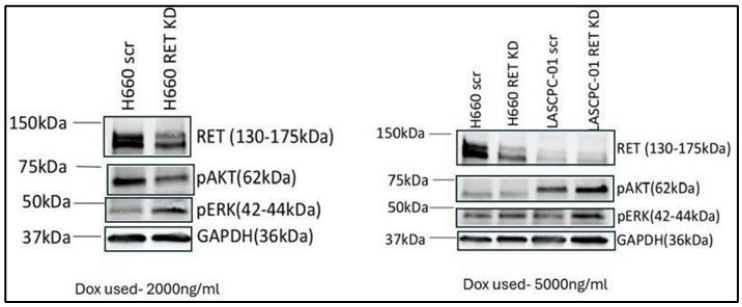

B

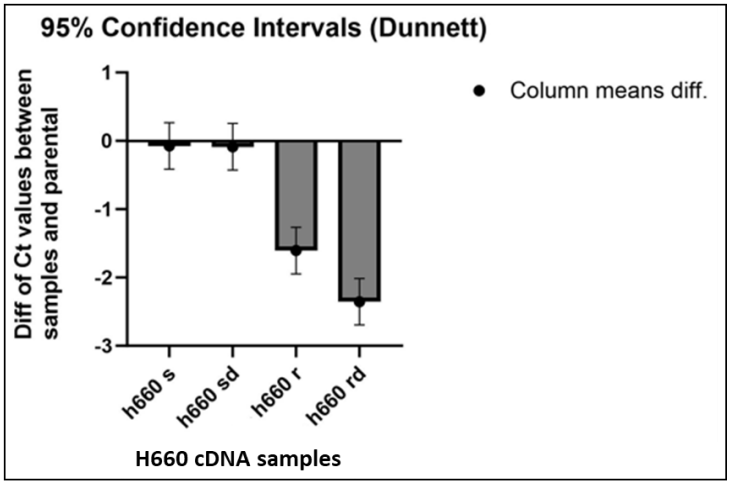

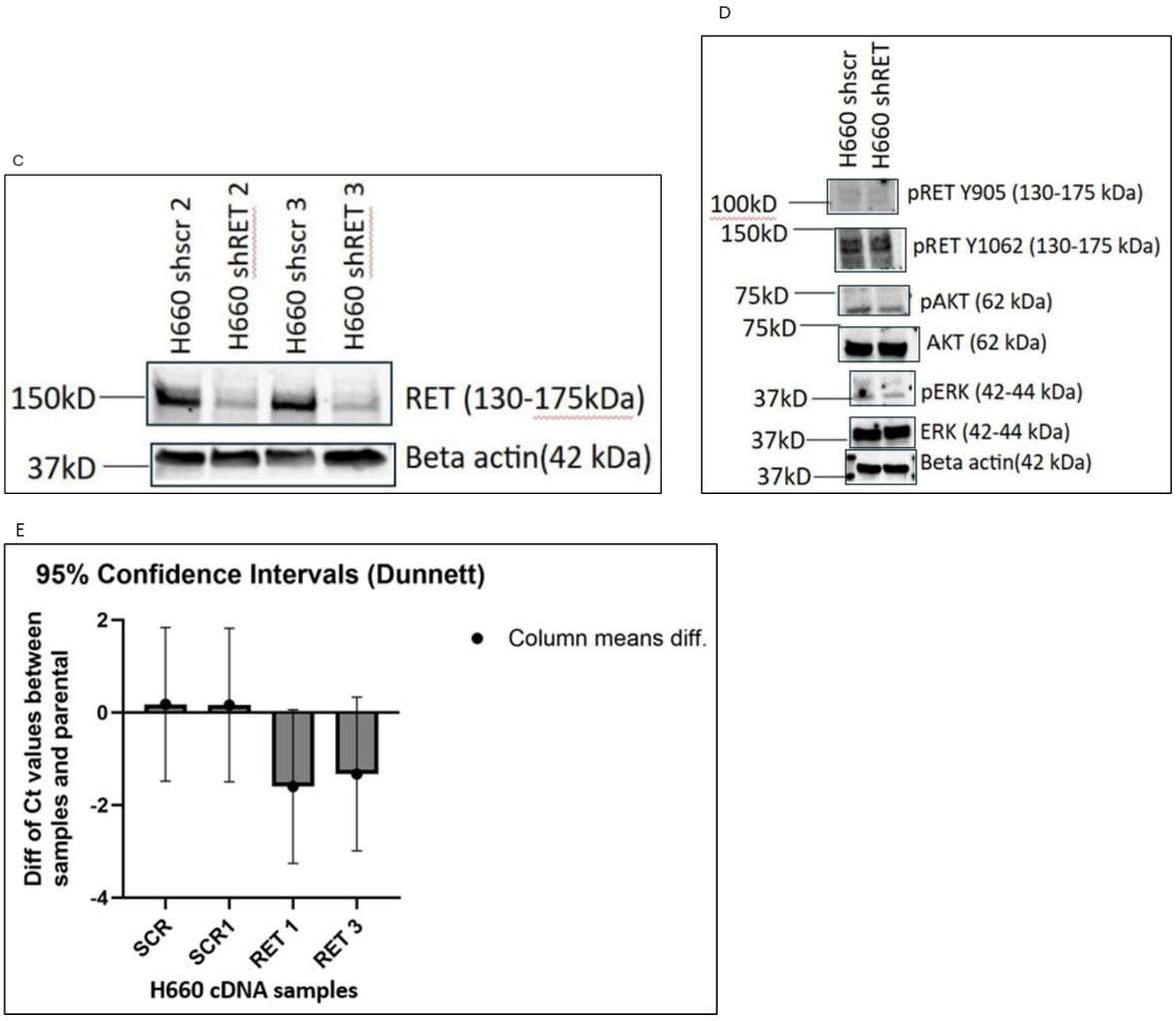

Figure 6: Cell line panel of prostate cancer cell line after knocking down RET. A. Western blot showing activation of RET and its downstream targets in doxycycline induced knockdown in H660 cell line. Doxycycline concentration of 5ug/mL used. B. qPCR data graphed on GraphPad Prism showing a linear graph of the difference of Ct values, with error bars representing the fold change standard deviation. H660 parental cDNA was compared to other samples and y axis corresponds to the different treatment conditions. h660s- H660 scrambled without doxycycline, h660sd- H660 scrambled with doxycycline, h660r- RET KD without doxycycline, h660rd- RET KD with doxycycline. C and D- Western blot of activation patterns of RET, phosphorylated RET, and other downstream targets after lentiviral transduction of shRET and using shscr as a control. E. qPCR data graphed on GraphPad Prism showing a linear graph of the difference of Ct values, with error bars representing the fold change standard

deviation. H660 parental cDNA was compared to other samples and y axis corresponds to the different treatment conditions. SCR and SCR1- scrambled controls. RET1 and RET3- RET KD treatments.

3.3 RNA QC data

In order to carry out RNA sequencing, RNA was isolated from the cell pellet and the isolated RNA was sent to figure out the RIN scores. The table below summarizes the scores of the samples that are going to be sent for analysis.

Cell line	RIN score
PC3 RET OE	9, 10, 9
PC3 GFP	10, 10, 10
H660 RET KD	10, 10, 10
H660 scr	10, 10, 9.8
SHP77 RET KD	In progress
SHP77 scr	In progress

Table 2: RIN scores of prostate and lung cancer cell lines.

CHAPTER II

Development of a RET- targeted

Antibody Drug Conjugate

SUB-CHAPTER I: Introduction

An antibody-drug conjugate (ADC) consists of a monoclonal antibody (mAb) chemically linked to a cytotoxic drug as shown in Fig 7. This structure harnesses the precise targeting capability of antibodies along with the powerful cell-killing effect of the attached drug, enabling the selective and efficient destruction of cancer cells.[30]

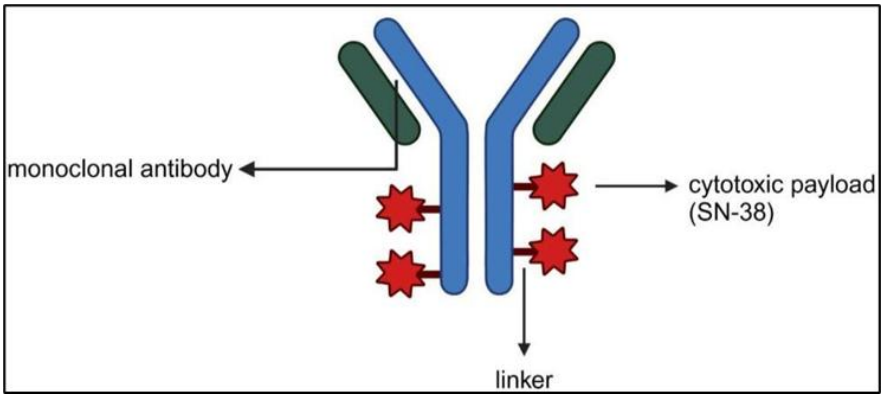

Figure 7: Structure of an ADC. Monoclonal antibody linked to the cytotoxic payload with the help of a linker.

As a result, ADCs have emerged as a key focus in anticancer drug research and development. Often referred to as "biological missiles," these innovative therapies are driving a new era in targeted cancer treatment. ADCs present a viable substitute for conventional chemotherapy by delivering cytotoxic medications to tumor cells selectively while reducing off-target effects, especially in cancers with distinct cell surface antigens.[31] ADCs consist of three key components. Monoclonal antibody (mAb) is made to precisely

identify and attach to a tumor-associated antigen (TAA) that is present in trace amounts in healthy tissues and ideally overexpressed on cancer cells. Linker is a chemical link between the cytotoxic payload and the antibody. Linkers can affect the drug's release mechanism inside the tumor cell by being cleavable (such as pH- sensitive, enzyme-sensitive, or reductive cleavage) or non-cleavable. Payload is usually a very strong cytotoxic substance that is toxic enough to be administered systemically, such as microtubule inhibitors or DNA-damaging substances.[32]

The ADC first attaches itself to its target antigen on the surface of the cancer cell, then it internalizes and moves to the lysosome. If the linker is cleavable, it is broken down in the acidic lysosomal environment, releasing the cytotoxic payload intracellularly. The drug's release then causes cell death by inducing apoptosis or cell cycle arrest. Fig 8 is the illustration of the mechanism of action of the ADC. Furthermore, certain ADCs have a bystander effect, which increases anticancer efficacy by allowing the payload to permeate into nearby tumor cells that might not express the target antigen.[33]

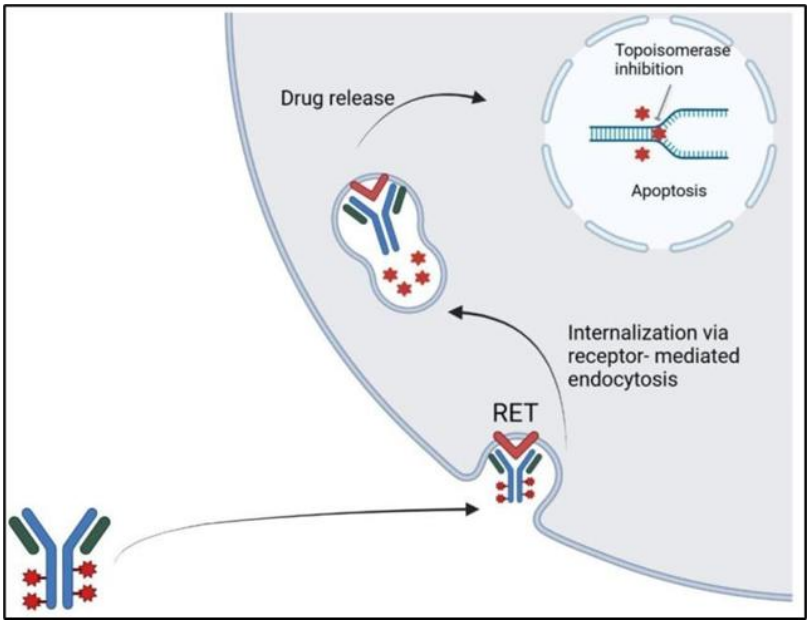

Figure 8: Mechanism of action of our RET-targeted ADC. ADC internalization into the cell is followed by lysosomal degradation after which the payload gets attached to the target leading to apoptosis.

The efficacy and safety of ADCs depend on multiple factors, such as antigen selection. To prevent on-target off-tumor damage, the optimal TAA should be missing or low in normal tissues, strongly expressed in tumor cells, and internalized effectively following antibody binding.

Linker stability: Linkers need to be both labile enough to guarantee effective payload release within the tumor cell and stable in circulation to avoid toxicities and premature drug release. Drug potency: Payloads need to be extremely potent (low nanomolar to picomolar IC_{50} values) because each antibody can conjugate to a certain number of drug molecules (usually 2–8). Drug-antibody ratio (DAR): An important characteristic that influences toxicity, effectiveness, and pharmacokinetics. Potency can be increased with more DAR, but stability and solubility may be jeopardized.[34] A powerful class of cytotoxic drugs, topoisomerase I inhibitors are especially well-suited as payloads in ADCs that target RET in NEPC. To cause irreversible double-strand breaks and apoptosis, topoisomerase I inhibitors, like the exatecan derivative SN-38, cause DNA damage during replication. These processes are particularly efficient in rapidly dividing cells like those in NEPC. Trastuzumab emtansine (T-DM1), trastuzumab deruxtecan (T-DXd), sacituzumab govitecan, and datopotamab deruxtecan are clinically approved antibody-drug conjugates (ADCs) that have significantly advanced targeted cancer therapy. T-DM1, approved for HER2-positive breast cancer, links trastuzumab to the cytotoxic microtubule inhibitor DM1 via a non-cleavable linker, enabling selective delivery of chemotherapy to HER2-expressing cells.[35] T-DXd, also

targeting HER2, employs a cleavable linker and a potent topoisomerase I inhibitor payload (deruxtecan), offering a bystander killing effect and showing efficacy even in HER2-low breast cancer. Sacituzumab govitecan targets Trop-2 and delivers SN-38, the active metabolite of irinotecan, via a hydrolysable linker and it is approved for triple-negative breast and urothelial cancers.[36] Datopotamab deruxtecan, currently in late phase trials, also utilizes deruxtecan but targets TROP2 with a novel optimized linker, showing promise in breast and lung cancers with a favorable toxicity profile compared to earlier ADCs.[37] These agents exemplify the evolution of ADC technology in enhancing therapeutic precision and overcoming resistance.

These inhibitors have the dual advantages of high efficacy and the capacity to cause a bystander-killing impact when used as ADC payloads. This is especially helpful given the tumor heterogeneity frequently seen in NEPC.[38] To address a significant unmet need in the treatment of advanced prostate cancers with neuroendocrine differentiation, a topoisomerase I inhibitor coupled to a RET-targeted ADC provides a guided approach to specifically eliminate RET-expressing neuroendocrine tumor cells while reducing systemic toxicity.

SUB-CHAPTER II: Materials and Methods

2.1 Bacterial Transformation and Culture Preparation

scFv plasmids (pET22b+ construct) 3 and 5 were designed by Halena VanDeusen., PhD, a former postdoc in our lab. We transformed the plasmids into competent *E. coli* T7 Shuffle strain using a heat-shock method. Transformed bacteria were plated on LB agar supplemented with ampicillin (100 µg/mL) and incubated overnight at 37°C. A single colony was picked and inoculated into 3–5 mL of LB broth containing ampicillin (100 µg/mL), followed by overnight incubation at 37°C with shaking at 220 rpm. Some of the cultures were used for DNA sequencing to verify the scFv sequences after isolating the plasmid.

2.2 Induction of scFv Expression

10mL from the overnight starter culture was diluted into 1 L of pre-warmed LB+ ampicillin and put on a shaker for 2 hours to reach an OD600 value of 0.6-0.8. Two separate cultures were prepared- one for IPTG induction and one as uninduced control. The cultures were incubated at 37°C with shaking until OD600 reached 0.6–0.8. Induction was initiated by adding IPTG to a final concentration of 0.5 mM, with incubation continued at 20°C for 24 hours (slow induction). The uninduced control was incubated under similar conditions without IPTG.

2.3 Periplasmic Extraction

The next day, bacterial cultures were harvested by centrifugation at 4,000 x g for 15 minutes. The pellet was resuspended in ice-cold osmotic shock buffer (50mM Tris-HCl, 20% sucrose, pH 7.2) and later incubated at room temperature 1 hour. The suspension was centrifuged at 10,000 × g for 10 minutes, and the supernatant was collected. Ice-cold Milli-Q water containing EDTA free protease inhibitor cocktail was added to the supernatant, followed by incubation on ice for 3 minutes. After performing a final centrifugation at 12,000 × g for 10 minutes, the supernatant containing periplasmic proteins was collected.

2.4 SDS-PAGE and Western Blot Analysis

Protein expression was analyzed by SDS-PAGE. Induced and uninduced culture supernatants were mixed with Laemmli sample buffer and heated at 95°C for 10 minutes. Samples were loaded onto an SDS-PAGE gel alongside an unstained protein ladder and separated by electrophoresis. Gels were imaged using a Chemi-Doc system under UV settings. For Western blot analysis, proteins were transferred onto a PVDF membrane, followed by a standard Western blot protocol as mentioned above using an anti-His antibody. RET scFvs were expected at ~26.5 kDa. For Coomassie stained blots, Coomassie Brilliant Blue R-250 by Biorad were used to stain the blots. After adding the stain, the blots were microwaved for 15 seconds followed by incubation at room temperature on a shaker for 15 minutes. Then a destaining solution was made using 50% ethanol, 10% glacial acetic acid and MilliQ water to get rid of the stain. The blot was then imaged using the Chemi-Doc system.

2.5 Dialysis to remove contaminating salts

The periplasmic proteins were loaded on a Spectra/Por® 1-5 Standard RC Dry Dialysis Trial Kits, Spectrum® Laboratories dialysis membrane, and released in a resuspension buffer of Phosphate-buffered saline (PBS). They were left overnight at 4 C on a magnetic shaker followed by another 4 hours shaking on the next day to remove EDTA and any other contaminating salts.

2.6 Purification of scFv using TALON Resin Column

The Cytiva Talon superflow resin was primed before sample application. Milli-Q water was passed through the column until the liquid level reached ~1 cm above the resin. 0.1 M EDTA at pH 8 was applied to chelate any unwanted metal ions, followed by Milli-Q water to remove excess EDTA. 0.1 M cobalt chloride was added to recharge the resin with cobalt ions. The column was washed again with Milli-Q water, followed by a resuspension buffer.

2.7 Protein Binding and Wash Steps

The clarified lysate containing periplasmic proteins was applied to the equilibrated TALON resin column and allowed to flow through by gravity. Fractions were collected at each step:

Flow-through fraction (FT) – Lysate that did not bind to the column.

Wash 1 – 25 mL resuspension buffer was applied to remove unbound proteins.

Wash 2 – 25 mL of resuspension buffer with 2 mM imidazole was added.

Wash 3 – 25 mL of resuspension buffer with 10 mM imidazole was added.

Wash 4– 25 mL of resuspension buffer with 40 mM imidazole was added.

Wash 5 – 25 mL of resuspension buffer with 150 mM imidazole was used for final purification.

Each wash fraction was collected and analyzed for protein content.

The fractions were then concentrated using Amicon Ultra Centrifugal filters with a molecular cutoff of 10kDa, spun at 3600xg for 20 minutes. The concentrated fractions were used for western level.

2.8 Coomassie blot and Western Blot Analysis

Protein expression and purification efficiency were analyzed by SDS-PAGE. Samples from each purification step were mixed with a 2× Laemmli sample buffer. Samples were loaded onto a gel alongside an unstained protein ladder and separated by electrophoresis. Gels were stained and imaged using a Chemi-Doc system. A similar protocol was followed for a western blot analysis to visualize the protein at ~26.5 kDa.

2.9 Flow cytometry

293T cells transfected to express wild-type RET were subjected to live-cell immunostaining for detection of surface RET binding to the RET domain on the scFv sequence and subsequent fluorescence-activated cell sorting (FACS).

Buffers and media:

- 2% FBS in PBS AND 2mM EDTA (prepared by dilution of the 10X stock)
- DMEM media with 1% glutamine, 1% penicillin/streptomycin, and 10% FBS.

- **Antibodies:**
    - Primary: Ret (E1N8X) XP® Rabbit monoclonal antibody (Cell Signaling Technology), recognizing the extracellular N-terminal domain of RET, was used as the positive control.
    - Primary: His Tag Antibody mAb Mouse (Genescript) which will bind to the histidine residues on the scFv.
    - Secondary: Goat anti-Rabbit IgG (H+L) Alexa Fluor 488-conjugated antibody (Invitrogen)
    - Secondary: Goat anti-Mouse IgG (H+L) Alexa Fluor 488-conjugated antibody (Invitrogen)
    - Secondary: propidium iodide live/dead stain (Invitrogen)

Cell Harvest and Blocking

Cells were trypsinized, harvested, and centrifuged at 300 × g for 5 minutes. The supernatant was discarded, and cells were resuspended in a growth medium. After counting, 2.5×10^5 cells were aliquoted into individual Eppendorf tubes according to experimental conditions. Cells were pelleted again (300 × g, 3 minutes), resuspended in 1X blocking buffer, and blocked for 30 minutes at room temperature on a rotator.

Immunostaining Procedure

Following blocking, cells were incubated with scFv for 1.5 hours at 4°C during the incubation period. After incubation, cells were washed thrice, pelleted and resuspended in 200 µL of

primary antibody diluted 1:200 in the flow buffer. Primary antibody incubation was carried out for 1 hour at 4°C with gentle rotation.

Cells were then washed three times with 1X PBS. Subsequently, cells were resuspended in 100 µL of the Alexa Fluor 647-conjugated secondary antibody diluted 1:1000 in flow buffer. Secondary antibody incubation was performed for 30 minutes at 4°C in the dark with gentle rotation.

Following incubation, cells were washed three more times with PBS as described above, then resuspended in 500 µL of 1:1000 dilution of the live/dead stain. The cell suspension was filtered through the cap of a FACS tube (Falcon 352235) and kept protected from light before analysis.

Flow Cytometric Analysis

Samples were analyzed and sorted using a BD FACSymphony A3 flow cytometer. Controls included unstained cells, cells stained with live/dead stain only, and RET single-stained samples (RET primary and secondary). Compensation was performed using appropriate controls for each fluorophore. Treatment included RET primary antibody, 10ug/ml of scFv along with primary His tagged antibody followed by secondary, and 360ug/mL with similar immunostaining. Cells were first gated on forward and side scatter to exclude debris, followed by singlet discrimination. PI positive and the Alexa Fluor 488 were gated for accurate compensation. Alexa Fluor 488 fluorescence was assessed to detect surface RET expressions.

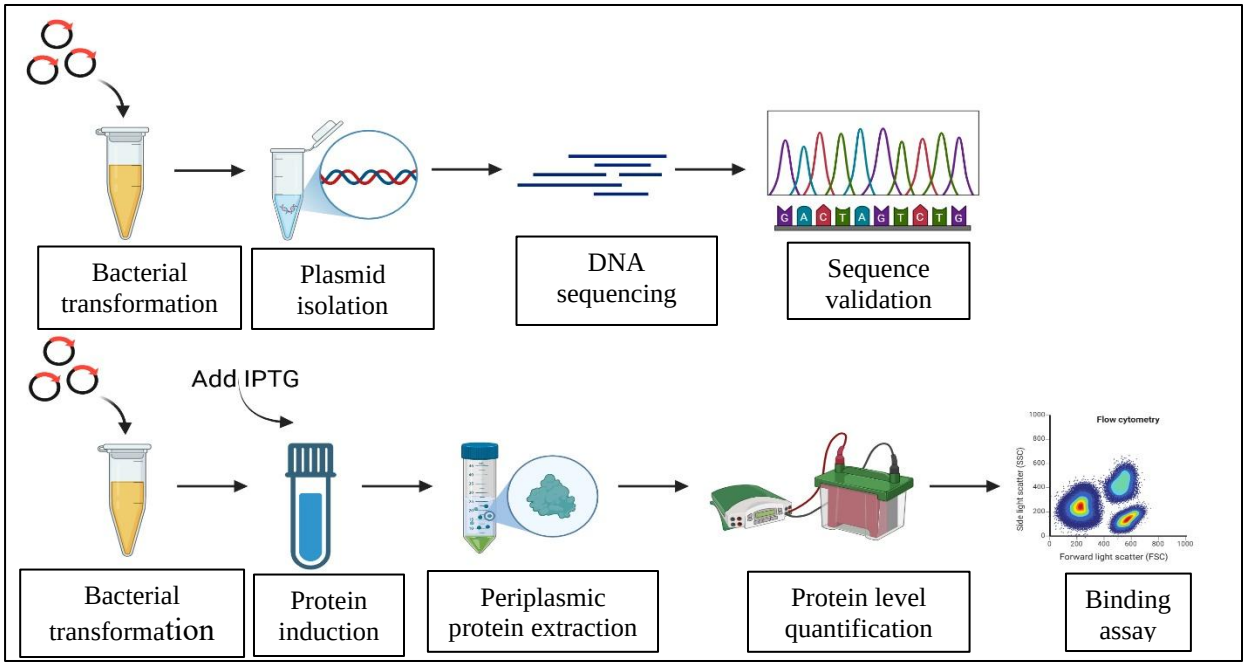

Figure 9: Experimental flow for the RET ADC project. The figure on the top shows bacterial transformation with NEB stable competent *E. coli* strain with the scFv plasmid followed by DNA sequencing to validate the sequences. The second figure shows the T7 shuffle strain of *E. coli* used for bacterial transformation for expression and binding studies. IPTG was used for protein induction. Talon column was used for purification followed by protein expression validation using western blots and Coomassie staining blots. Finally, flow cytometry was used for binding assay on RET-positive cell lines and RET-negative cell lines were used as controls.

SUB-CHAPTER III: Results

3.1 DNA sequencing results validated the scFv sequences

Using NCBI BLAST we cross-checked the DNA sequencing results by ACGT with the plasmid sequences that were used to prepare the plasmids. Out of the 2 plasmids that were tested, the scFv 5 had a linker missing while the scFv 3 was unchanged. This could be attributed to homologous recombination in the *E coli* strain. Since the part of the sequence that binds to the extracellular domain of RET was intact, we went ahead with both the plasmids for protein production and binding studies.

3.2 Inducing proteins in the bacteria using IPTG and periplasmic extraction

For protein induction different temperature conditions and concentrations of IPTG were tested ranging from 0.1- 5mM. After testing multiple conditions, a slow induction with 0.5mM IPTG and slow induction for 18- 20 hours at 20℃ gave the best results with the least amount of degradation product. To extract the periplasmic protein by breaking the periplasm layer, an osmotic shock buffer was used. Different concentrations of Tris-HCl, sucrose, and EDTA were tested and optimized. Finally, we went ahead with 50 mM Tris and 20% sucrose at a pH of 7.2. We also used an EDTA-free protease inhibitor.

3.3 Coomassie stain and Western blot to visualize the induced protein

We first tried to visualize the protein using SDS PAGE but due to specificity issues, an evident band was not visible. We then switched to Coomassie stains and western blots using an anti-

His antibody to visualize the protein. A band was seen at the desired molecular weight. To further purify the protein before loading it on a Talon column, dialysis was done for 36 hours to ensure the complete removal of EDTA and other unwanted salts. After purifying and collecting different fractions of our desired protein and concentrating it, we visualized it using Coomassie and Western blot. Fig 10 and 11. 10A, 11A, and 10B, 11B display RET scFv 3 and 5, respectively.

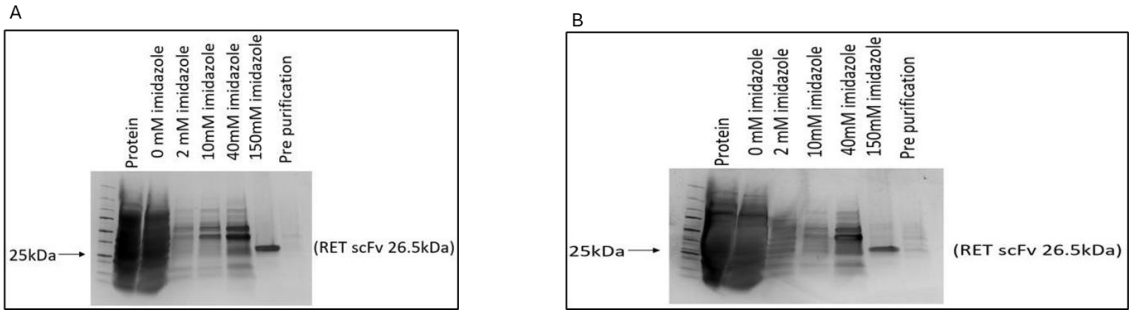

Figure 10: Coomassie stain blots for scFv visualization. His-Tagged protein expression seen at 26.5kDa.

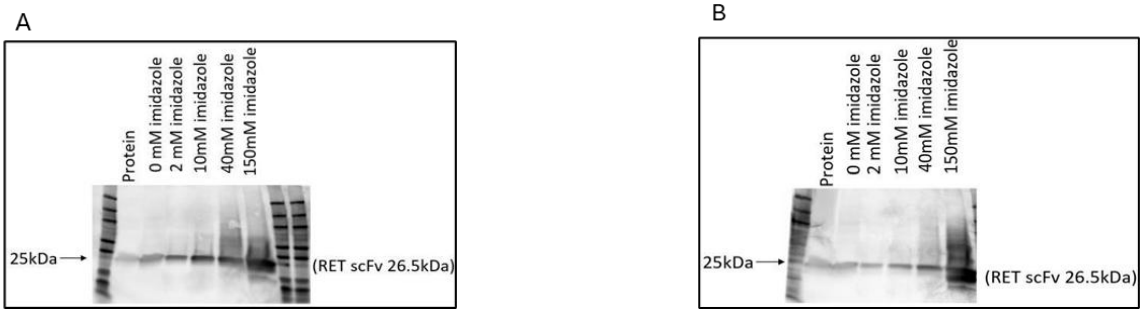

Figure 11: Western blots for scFv visualization using His-Tagged antibody. His-Tagged protein expression seen at 26.5kDa.

3.4 Flow cytometry and Flowjo analysis

To evaluate the surface expression of RET in live 293T RET overexpressed cells, we performed flow cytometry analysis using an immunostaining approach targeting the extracellular domain of RET. Cells were incubated with the scFv and then the unconjugated antibody, followed by staining with a fluorescently labeled secondary antibody. Since the scFv had a His- segment, a His Tagged antibody was used to determine the percentage of binding. Cells were incubated with the ADC at 10 ug/mL and 360 ug/ml concentration for 1 hour at 4°C to prevent internalization. On FlowJo, the L/D compensation control was used to set the gates. A dot plot was used to gate the cells after which histogram plots depicted live cells and the cells that showed binding to our scFv, respectively. A distinct RET+ population was observed in the 293T RET overexpression group in the form of a rightward shift, indicating successful surface expression and antibody binding as seen in Figure 12. No significant signal was detected in the negative control as well as the compensation control groups, confirming the specificity of the RET binding. The binding was comparable in both the concentrations used. This suggests receptor saturation or other technical considerations.

These results demonstrate the feasibility of detecting extracellular RET in live, non-permeabilized 293T cells using antibody-based flow cytometry and support the use of this approach for binding our scFv to RET-positive cells.

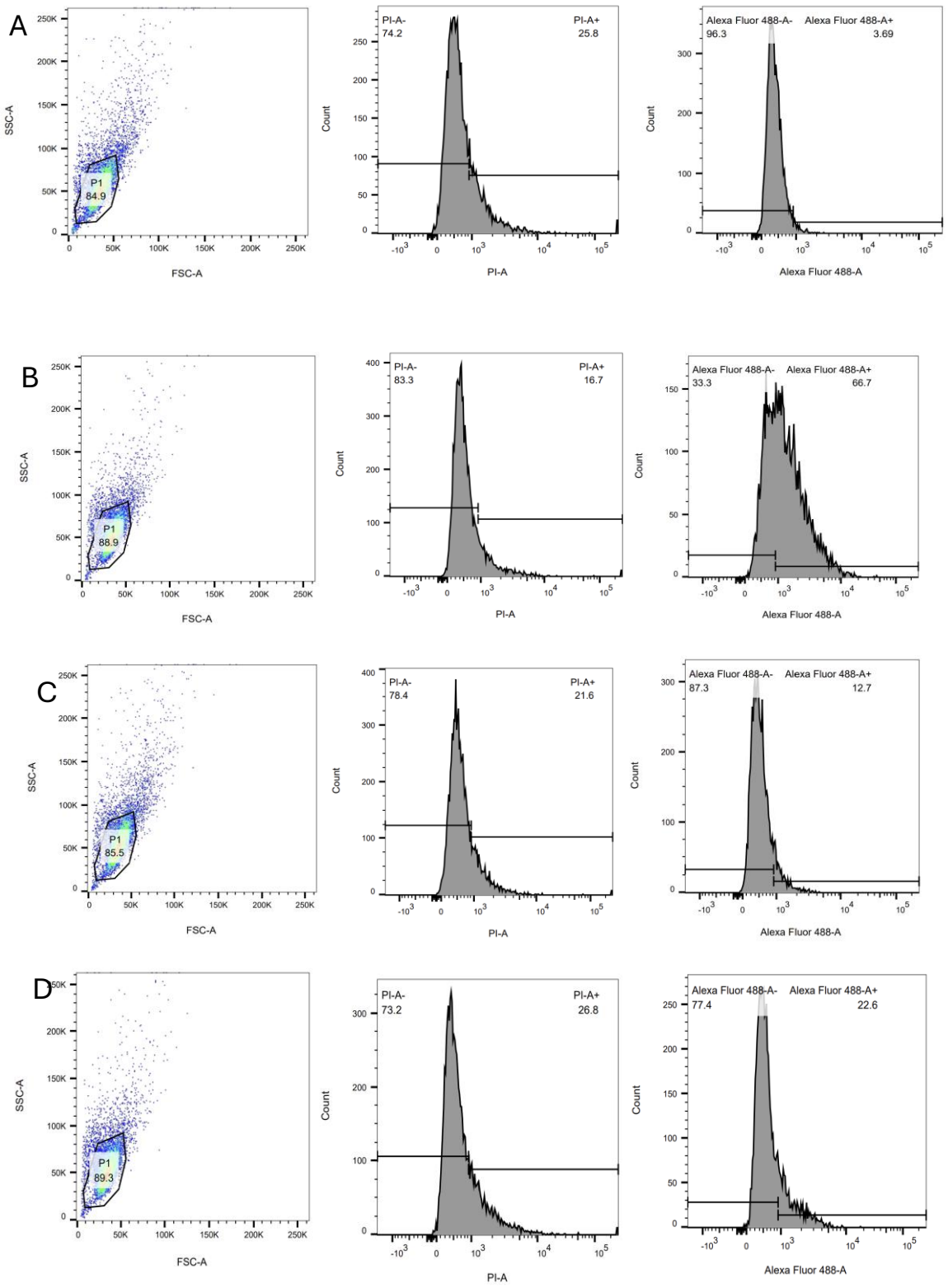
A
SSC-A
FSC-A
P1
84.9
PI-A-
74.2
PI-A+
25.8
Count
PI-A
Alexa Fluor 488-A-
96.3
Alexa Fluor 488-A+
3.69
Alexa Fluor 488-A
B
P1
88.9
PI-A-
83.3
PI-A+
16.7
Alexa Fluor 488-A-
33.3
Alexa Fluor 488-A+
66.7
C
P1
85.5
PI-A-
78.4
PI-A+
21.6
Alexa Fluor 488-A-
87.3
Alexa Fluor 488-A+
12.7
D
P1
89.3
PI-A-
73.2
PI-A+
26.8
Alexa Fluor 488-A-
77.4
Alexa Fluor 488-A+
22.6

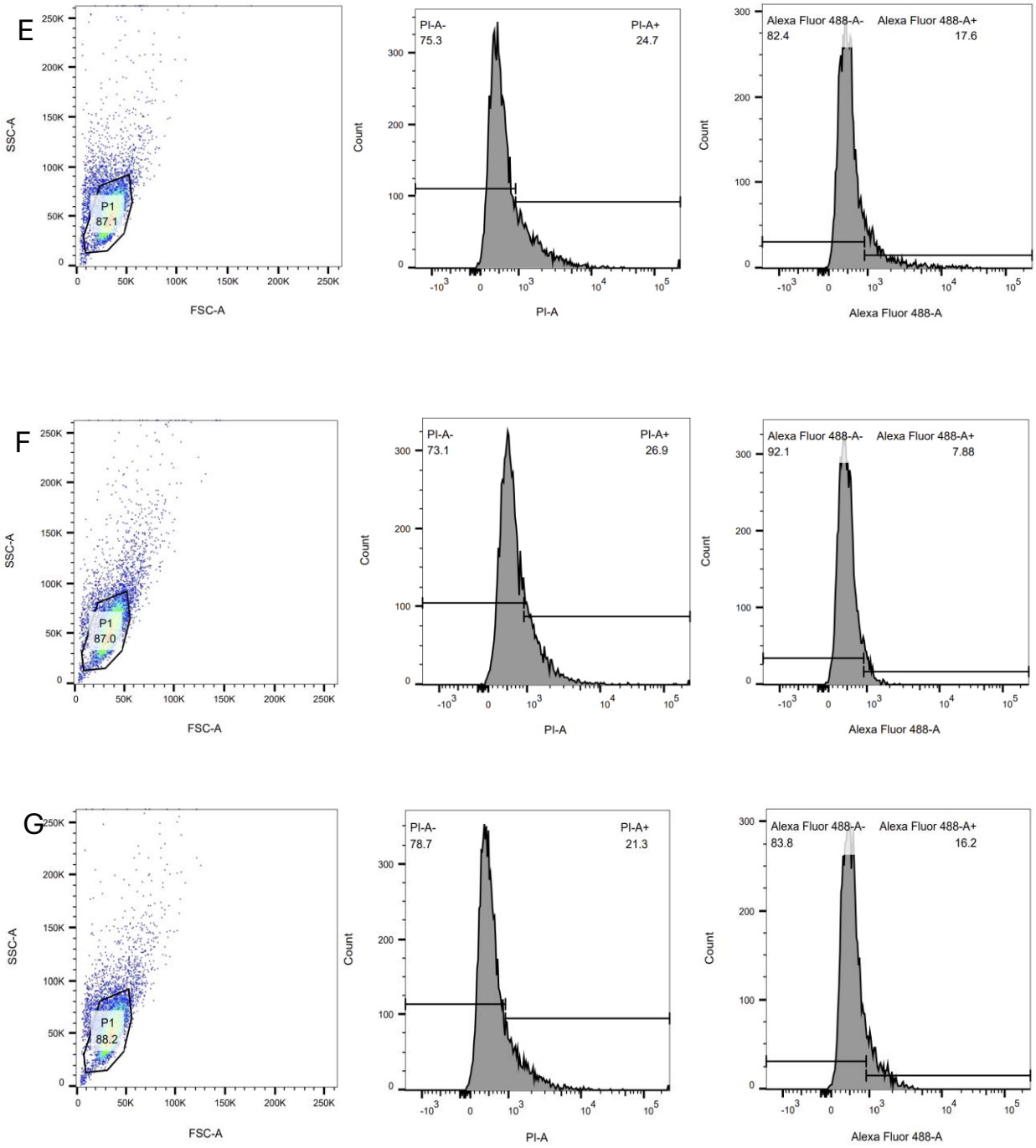
E
SSC-A
FSC-A
P1
87.1
Count
PI-A
PI-A-
75.3
PI-A+
24.7
Alexa Fluor 488-A
Alexa Fluor 488-A-
82.4
Alexa Fluor 488-A+
17.6
F
P1
87.0
PI-A-
73.1
PI-A+
26.9
Alexa Fluor 488-A-
92.1
Alexa Fluor 488-A+
7.88
G
P1
88.2
PI-A-
78.7
PI-A+
21.3
Alexa Fluor 488-A-
83.8
Alexa Fluor 488-A+
16.2

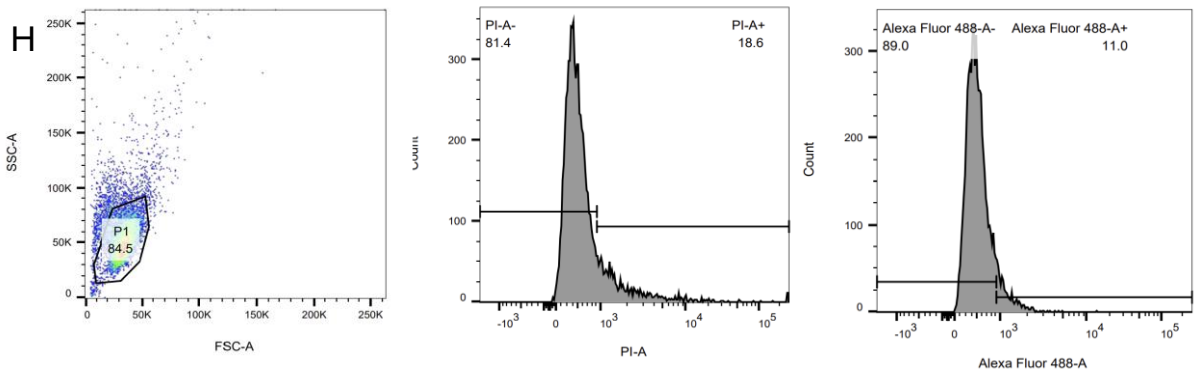

Figure 12: Flow cytometry results to show binding between HEK 293T cells and the scFv 3 and 5. A. HEK293T parental cells are stained with RET primary antibody Negative Control. B. HEK293T RET overexpressed cells stained with RET primary antibody Positive Control. C. HEK293T parental cells stained with His Tagged antibody after incubation with scFv 3 (10ug/ml). D. HEK293T RET overexpressed cells stained with His Tagged antibody after incubation with scFv 3 (10ug/ml). E. HEK293T RET overexpressed cells stained with His Tagged antibody after incubation with scFv 3 (360ug/ml). F. HEK293T parental cells stained with His Tagged antibody after incubation with scFv 5 (10ug/ml). G. HEK293T RET overexpressed cells stained with His Tagged antibody after incubation with scFv 5 (10ug/ml). H. HEK293T RET overexpressed cells stained with His Tagged antibody after incubation with scFv 5 (360ug/ml).

CHAPTER III

DISCUSSION

NEPC remains a significant clinical challenge due to its aggressive nature, poor prognosis, and resistance to conventional androgen deprivation therapies. Given the increasing prevalence of NEPC as a treatment-emergent phenotype in mCRPC, there is an urgent need for novel targeted therapeutics. In this study, we investigated the impact of RET overexpression and knockdown on lung and prostate cancer cell lines to define an mRNA-based signature associated with RET signaling. RET, a receptor tyrosine kinase, has been implicated in various malignancies, but its role in cell lines lacking endogenous expression remains unclear.

Our findings suggest that forced overexpression of RET in RET-negative cell lines may induce distinct transcriptional changes, potentially activating downstream oncogenic pathways. These results highlight the potential oncogenic influence of RET in contexts where it is not naturally expressed.

Conversely, RET knockdown in cell lines with endogenous RET expression did not lead to significant downregulation of known key oncogenic pathways, including MAPK/ERK and PI3K/AKT signaling. The comparison of transcriptomic signatures between RET-overexpressing and RET-knockdown conditions will potentially allow us to identify a set of differentially expressed genes that may serve as a RET-associated mRNA signature. This signature could be valuable in predicting RET dependency and response to RET-targeted therapies in clinical settings. Future studies should focus on validating this signature in patient-derived samples and assessing its prognostic and therapeutic relevance.

Overall, our findings will underscore the significance of RET signaling in lung and prostate cancer, particularly in cases where RET expression is altered. These results provide a

foundation for further exploration of RET as a potential biomarker and therapeutic target in these malignancies. The second half of this study proposes a RET-targeted ADC linked to the potent cytotoxic agent SN-38 as a promising strategy to address NEPC. Our approach is supported by previous findings that RET is overexpressed in NEPC. The selective targeting of RET ensures a focused therapeutic strategy with potentially minimal off-target effects. This specificity is crucial in the ADC framework, as it allows for the targeted delivery of cytotoxic agents while minimizing systemic toxicity. Notably, while RET-ADCs have been explored in different cancer models, their application in NEPC remains untested. Our study seeks to bridge this gap by evaluating the efficacy of RET-ADC in NEPC models.

Our research strategy involved the optimization of RET-binding single-chain fragment variables (scFvs), ensuring high specificity. Additionally, the selection of SN-38 as the payload represents a strategic decision, given its efficacy in neuroendocrine malignancies and potential activity in chemotherapy-resistant models.

Preliminary findings suggest that RET-ADC exhibits binding with RET-positive NEPC cells compared to RET-negative controls. These results validate our hypothesis that RET-ADC could be an effective treatment strategy for NEPC. This study introduces RET-ADC as a novel therapeutic strategy for NEPC, leveraging the selective expression of RET in this aggressive prostate cancer subtype. The promising in vitro results highlight the potential of ADC-based therapies in NEPC and underscore the necessity for further preclinical development. As the field of ADCs continues to evolve, optimizing targeting strategies and payload-linker combinations will be key to maximizing therapeutic efficacy while minimizing toxicity. Our findings

contribute to the growing body of research focused on developing precision medicine approaches for lethal prostate cancer.

CHAPTER IV

FAILED EXPERIMENTS AND TROUBLESHOOTING

A wildtype shRET knockdown was tried on the small cell lung cancer cell lines SHP77 and DMS53 which did not work as shown in Fig 13 A and B. Next, siRNA was used along with lipofectamine RNAiMAX by Thermo Fisher as the transfection agent. siRNA was ordered by IDT. We plated 3 x 10^5 cells a day before transfection. 293T RET overexpressed cells were used as the control and the transient knockdown was used on SHP77 and DMS53 cell lines. Since the 10nM of siRNA did not give any knockdown as seen in Fig 14A, the siRNA concentration was increased to 30nM. The isolates were collected after 24 hours and later 72 hours as seen in Fig 14 B and C. Fig 15 represents western blots after transfecting the lung cancer cells using shRNA vector and TransIT-LT1 by Millipore Sigma as the transfection reagent. 5 x 10^5 cells were plated for transfection and 2.5 ug from a 1ug/ul stock of the plasmid DNA was used.

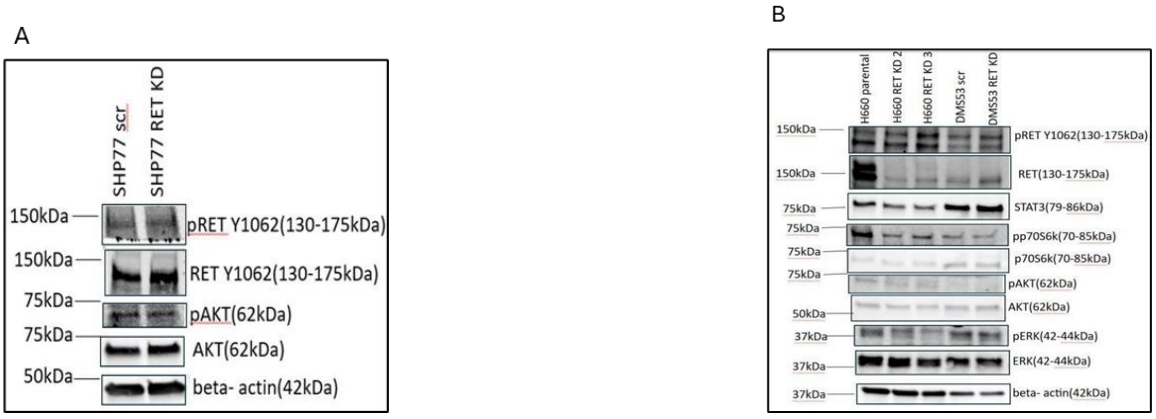

Figure 13: Wild-type shRNA transduction in DMS53 and SHP77. A and B. Western blot showing shRET knockdown in SCLC cell lines SHP77 and DMS53. H660 knockdown was used as a positive control. shRNA scrambled was a negative transduction control and beta-actin was the loading control.

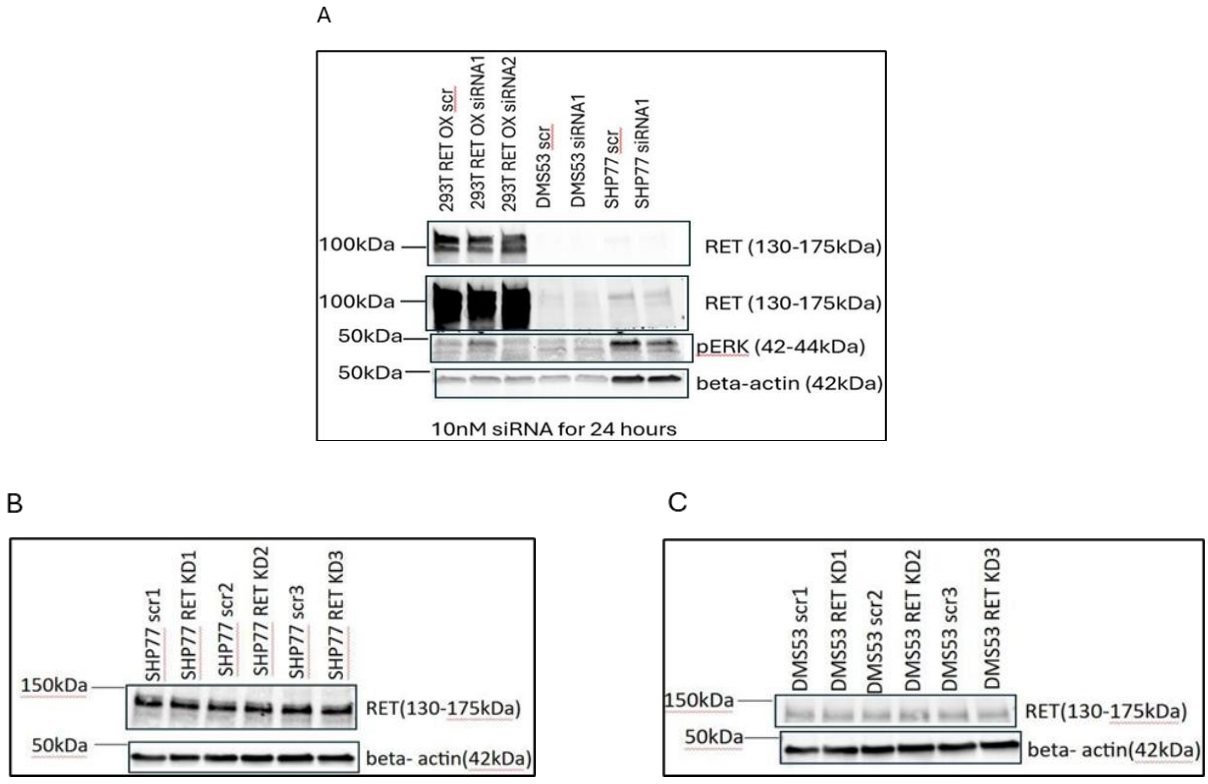

Figure 14: siRNA transfection SCLC cell lines SHP77 and DMS53 using lipofectamine. HEK 293T was used as a positive transfection control.

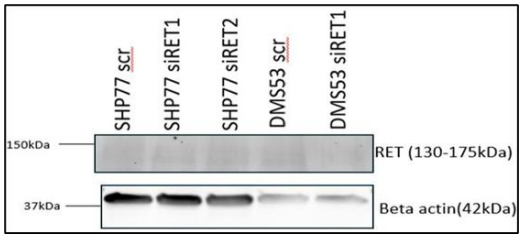

Figure 15: **siRNA transfection in SCLC cell lines SHP77 and DMS53 using TransIT**

For the ADC project, we first started the protein induction by using 5mM of IPTG followed by a fast induction at 37C for 4 hours. Fig 16 shows the SDS PAGE blot for the above-mentioned conditions. The estimated weight of our scFv is ~26.5kDa. We tried to optimize the concentration for IPTG but protein expression remained constant, regardless of the concentrations of IPTG used as shown in Fig 17A and B which represent scFv 3 and 5, respectively. The protein expression was more evident after carrying out western blots and using the His-Tagged antibody as shown in Fig 18. Slow induction works best with the least amount of degradation. We tried to optimize the osmotic buffer solution to eliminate the EDTA which will interfere with the column purification. We got the highest protein levels using 50mM Tris-HCl, 20% sucrose at pH7.2 which is represented in Fig 19A and B.

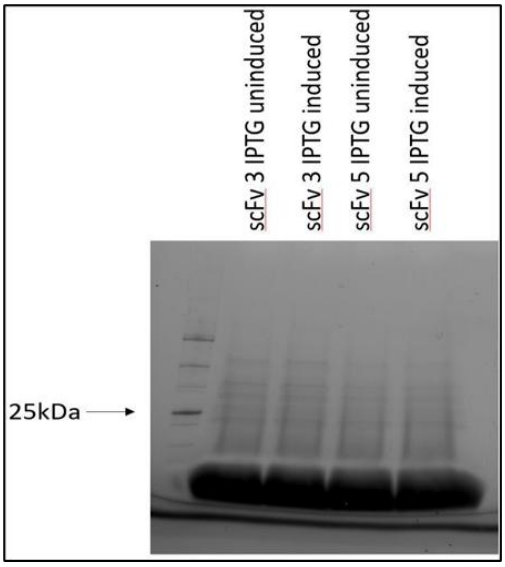

Figure 16: SDS PAGE after fast IPTG induction

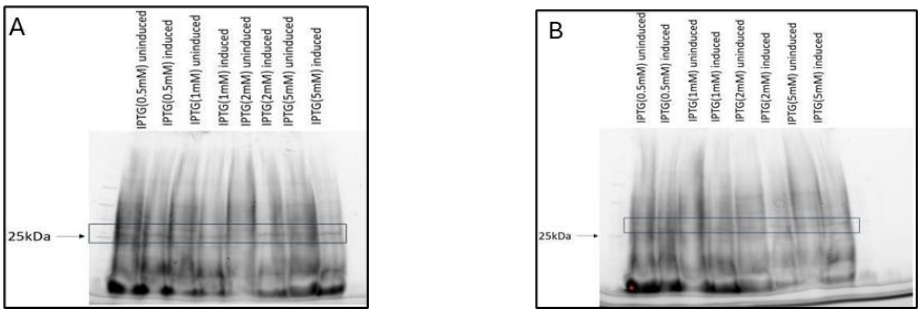

Figure 17: SDS PAGE showing induction using different IPTG ranges

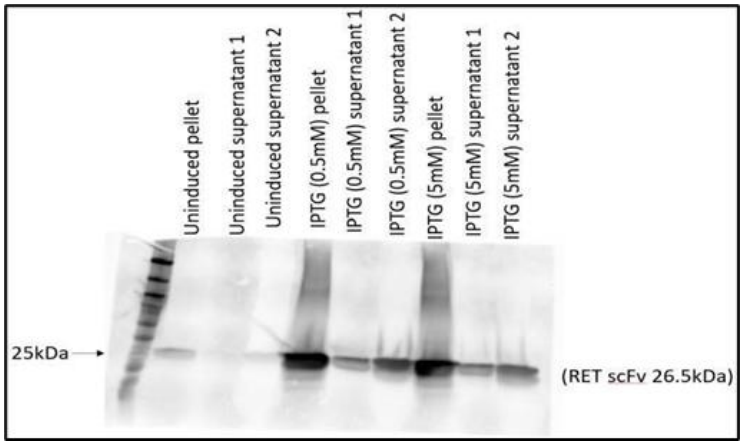

Figure 18: Western blot after slow IPTG induction

A

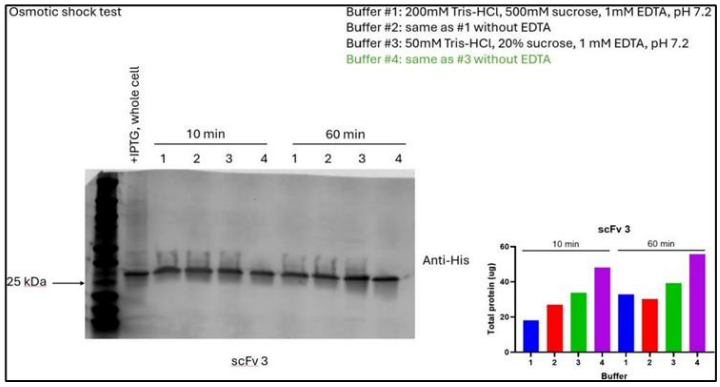

B

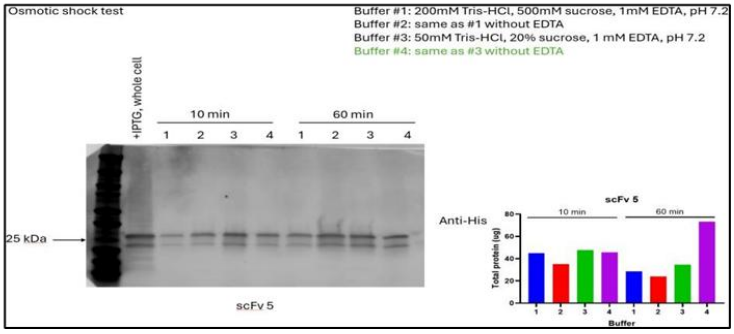

Figure 19: Western blot quantification to optimize osmotic shock buffer (By Megan)

CHAPTER V: FUTURE DIRECTIONS

After knocking down RET in SHP77 using shRET doxycycline inducible system, the samples will be sent to Novogene for mRNA sequencing where they will carry out an mRNA library preparation and a paired end sequencing, and provide us with the raw read counts. This data will then be analyzed by Dr. Justin Hwang's laboratory at the University of Minnesota to carry out a differential gene expression analysis to compare the RET overexpression/RET knockdown samples to the controls to see which genes are enriched. After figuring out the genes, RET will be overexpressed back in the knockdown samples and a qPCR will be carried out in parallel between both sets to figure out whether the genes that were knocked down are expressed again after RET overexpression. Gene set enrichment analysis will be done to elucidate the biological pathways controlled by RET expression in these NEPC cell lines. Since the end goal is to figure out whether this gene signature will be able to determine which subset of patients will benefit from RET inhibition therapies, RET inhibitors such as selpercatinib and pralsetinib might also be used in tumor models to verify the reduction in tumor growth and the decline in activation of RET and its dependent targets in patient samples.

For the ADC binding studies using flow cytometry, increased amounts of incubation and concentration with the primary antibody might give better binding results. Performing a binding curve using serial dilutions of the scFv might help to understand what concentration works best. After determining a good percentage of binding of the RET-positive cells with the scFv, we will focus on cleaving the His Tag in our construct for downstream purification using protease cleavage. We will also investigate the bystander effect, stability, and expression optimization of the construct. Dr. Daniel Harki's laboratory at the University of Minnesota

will help in linking our scFv construct to the topoisomerase inhibitor SN-38 using a cleavable linker. Further, downstream conjugation validation and cytotoxicity assays will be performed to ensure the functionality of our ADC.

Bibliography

1 Siegel, R. L., Kratzer, T. B., Giaquinto, A. N., Sung, H. & Jemal, A. Cancer statistics, 2025. *CA: A Cancer Journal for Clinicians* 75, 10-45, doi:10.3322/caac.21871 (2025).

2 Rawla, Prashanth. “Epidemiology of Prostate Cancer.” World Journal of Oncology, vol. 10, no. 2, Apr. 2019, pp. 63–89. PubMed, doi:10.14740/wjon1191.

3 Kang, J. *et al.* Tumor microenvironment mechanisms and bone metastatic disease progression of prostate cancer. *Cancer Letters* 530, 156-169, doi:10.1016/j.canlet.2022.01.015 (2022).

4 Tomlins, S. A. *et al.* Recurrent Fusion of TMPRSS2 and ETS Transcription Factor Genes in Prostate Cancer. *Science* 310, 644-648, doi:doi:10.1126/science.1117679 (2005).

5 Koh, C. M. *et al.* MYC and Prostate Cancer. *Genes & Cancer* 1, 617-628, doi:10.1177/1947601910379132 (2010).

6 Grasso, C. S. *et al.* The mutational landscape of lethal castration-resistant prostate cancer. *Nature* 487, 239-243, doi:10.1038/nature11125 (2012).

7 Chen, C. D. *et al.* Molecular determinants of resistance to antiandrogen therapy. *Nature Medicine* 10, 33-39, doi:10.1038/nm972 (2004).

8 Antonarakis, E. S., Armstrong, A. J., Dehm, S. M. & Luo, J. Androgen receptor variant-driven prostate cancer: clinical implications and therapeutic targeting. *Prostate Cancer and Prostatic Diseases* 19, 231-241, doi:10.1038/pcan.2016.17 (2016).

9 Aurilio, G. *et al.* Androgen Receptor Signaling Pathway in Prostate Cancer: From Genetics to Clinical Applications. *Cells* 9, 2653 (2020).

10 Wang, Y. *et al.* Molecular events in neuroendocrine prostate cancer development. *Nature Reviews Urology* 18, 581-596, doi:10.1038/s41585-021-00490-0 (2021).

11 Conteduca, V. *et al.* Clinical features of neuroendocrine prostate cancer. *European Journal of Cancer* 121, 7-18, doi:10.1016/j.ejca.2019.08.011 (2019).

12 Beltran, H. *et al.* Molecular Characterization of Neuroendocrine Prostate Cancer and Identification of New Drug Targets. *Cancer Discovery* 1, 487-495, doi:10.1158/2159-8290.Cd-11-0130 (2011).

13 Dardenne, E. *et al.* N-Myc Induces an EZH2-Mediated Transcriptional Program Driving Neuroendocrine Prostate Cancer. *Cancer Cell* 30, 563-577, doi:10.1016/j.ccell.2016.09.005 (2016).

14 Aparicio, A. M. *et al.* Combined Tumor Suppressor Defects Characterize Clinically Defined Aggressive Variant Prostate Cancers. *Clinical Cancer Research* 22, 1520-1530, doi:10.1158/1078-0432.Ccr-15-1259 (2016).

15 Yamada, Y. & Beltran, H. Clinical and Biological Features of Neuroendocrine Prostate Cancer. *Current Oncology Reports* 23, 15, doi:10.1007/s11912-020-01003-9 (2021).

16 Addeo, A. *et al.* RET aberrant cancers and RET inhibitor therapies: Current state-of-the-art and future perspectives. *Pharmacology & Therapeutics* 242, 108344, doi:10.1016/j.pharmthera.2023.108344 (2023).

17 Beltran, H. *et al.* Aggressive variants of castration-resistant prostate cancer.

18 VanDeusen, H. R. *et al.* Targeting RET Kinase in Neuroendocrine Prostate Cancer. *Molecular Cancer Research* 18, 1176-1188, doi:10.1158/1541-7786.MCR-19-1245 (2020).

19 Gainor, J. F. *et al.* Molecular Mechanisms of Resistance to First- and Second-Generation ALK Inhibitors in ALK-Rearranged Lung Cancer. *Cancer Discovery* 6, 1118-1133,

doi:10.1158/2159-8290.Cd-16-0596 (2016).

20 Drilon, A. *et al.* Efficacy of Selpercatinib in RET Fusion–Positive Non–Small-Cell Lung Cancer. *New England Journal of Medicine* 383, 813-824, doi:doi:10.1056/NEJMoa2005653 (2020).

21 Subbiah, V. *et al.* Selective RET kinase inhibition for patients with RET-altered cancers. *Annals of Oncology* 29, 1869-1876, doi:10.1093/annonc/mdy137 (2018).

22 Megyesfalvi, Z. *et al.* Clinical insights into small cell lung cancer: Tumor heterogeneity, diagnosis, therapy, and future directions. *CA: A Cancer Journal for Clinicians* 73, 620-652, doi:10.3322/caac.21785 (2023).

23 Meijer, J.-J. *et al.* Small cell lung cancer: Novel treatments beyond immunotherapy. *Seminars in Cancer Biology* 86, 376-385, doi:10.1016/j.semcancer.2022.05.004 (2022).

24 Yang, S., Zhang, Z. & Wang, Q. Emerging therapies for small cell lung cancer. *Journal of Hematology & Oncology* 12, 47, doi:10.1186/s13045-019-0736-3 (2019).

25 Su, P.-L. *et al.* DLL3-guided therapies in small-cell lung cancer: from antibody-drug conjugate to precision immunotherapy and radioimmunotherapy. *Molecular Cancer* 23, 97, doi:10.1186/s12943-024-02012-z (2024).

26 Sen, T. *et al.* Emerging advances in defining the molecular and therapeutic landscape of small-cell lung cancer. *Nature Reviews Clinical Oncology* 21, 610-627, doi:10.1038/s41571-024-00914-x (2024).

27 Molina, J. R., Yang, P., Cassivi, S. D., Schild, S. E. & Adjei, A. A. Non-Small Cell Lung Cancer: Epidemiology, Risk Factors, Treatment, and Survivorship. *Mayo Clinic Proceedings* 83, 584-594, doi:10.4065/83.5.584 (2008).

28 Liu, L., Soler, J., Reckamp, K. L. & Sankar, K. Emerging Targets in Non-Small Cell Lung Cancer. *International Journal of Molecular Sciences* 25, 10046 (2024).

29 Brown, S., Banfill, K., Aznar, M. C., Whitehurst, P. & Faivre Finn, C. The evolving role of radiotherapy in non-small cell lung cancer. *British Journal of Radiology* 92, doi:10.1259/bjr.20190524 (2019).

30 Maecker, H., Vidya, J., Sunil, B., Vasu, J. & and Junutula, J. R. Exploration of the antibody–drug conjugate clinical landscape. *mAbs* 15, 2229101, doi:10.1080/19420862.2023.2229101 (2023).

31 Fu, Z., Li, S., Han, S., Shi, C. & Zhang, Y. Antibody drug conjugate: the "biological missile" for targeted cancer therapy. *Signal Transduction and Targeted Therapy* 7, 93, doi:10.1038/s41392-022-00947-7 (2022).

32 Jin, Y., Schladetsch, M. A., Huang, X., Balunas, M. J. & Wiemer, A. J. Stepping forward in antibody-drug conjugate development. *Pharmacology & Therapeutics* 229, 107917, doi:10.1016/j.pharmthera.2021.107917 (2022).

33 Hafeez, U., Parakh, S., Gan, H. K. & Scott, A. M. Antibody–Drug Conjugates for Cancer Therapy. *Molecules* 25, 4764 (2020).

34 Pommier, Y. & Thomas, A. New Life of Topoisomerase I Inhibitors as Antibody–Drug Conjugate Warheads. *Clinical Cancer Research* 29, 991-993, doi:10.1158/1078-0432.Ccr-22-3640 (2023).

35 Minckwitz, G. v. *et al.* Trastuzumab Emtansine for Residual Invasive HER2-Positive Breast Cancer. *New England Journal of Medicine* 380, 617-628, doi:doi:10.1056/NEJMoa1814017 (2019).

36 Modi, S. *et al.* Trastuzumab Deruxtecan in Previously Treated HER2-Low Advanced Breast Cancer. *New England Journal of Medicine* 387, 9-20, doi:doi:10.1056/NEJMoa2203690 (2022).

37 Bardia, A. *et al.* Datopotamab Deruxtecan in Advanced or Metastatic HR+/HER2– and Triple-Negative Breast Cancer: Results From the Phase I TROPION-PanTumor01 Study. *Journal of Clinical Oncology* 42, 2281-2294, doi:10.1200/jco.23.01909 (2024).

38 Han, S. *et al.* The Potential of Topoisomerase Inhibitor-Based Antibody–Drug Conjugates. *Pharmaceutics* 14, 1707 (2022).